Electrochimica Acta 432 (2022) 141174

Contents lists available at ScienceDirect

Electrochimica Acta

journal homepage: www.journals.elsevier.com/electrochimica-acta

Investigation of the diffusion phenomena in lithium-ion batteries with distribution of relaxation times

Yulong Zhao *, Simon Kücher, Andreas Jossen

Chair for Electrical Energy Storage Technology, Department of Energy and Process Engineering, School of Engineering and Design, Technical University of Munich, Arcisstrasse 21, Munich, Bavaria 80333, Germany

ARTICLE INFO

Keywords:
Lithium-ion battery
Electrochemical impedance spectroscopy
Physics-based model
Distribution of relaxation times
Diffusion

ABSTRACT

The distribution of relaxation times method (DRT) has been widely used to quantify the numbers and characterize the properties of the physico-chemical processes inside the Li-ion battery (LIB). While most of the published works focused on the mid-high frequency range, the processes in the low frequency area, such as diffusion, have garnered less attention. The difficulties of applying the DRT to the diffusion processes include the more complicated mathematical treatment involved, the unknown influence of the porous electrode on the DRT spectra and the evaluation of the measured impedance with the developed theory. The galvanostatic intermittent titration technique (GITT) has been widely applied to determine the solid diffusion coefficient for the LIB. However, the GITT does not consider the geometry of the active material particles and cannot effectively separate the contribution of the solid diffusion from other processes, such as liquid diffusion. In the present work, a comprehensive theory is developed to investigate the DRT spectra of a LIB with a physics-based impedance model. Furthermore, an analytical expression is developed for the DRT spectra and analyzed in detail. The developed theory can help to determine the solid phase diffusion coefficient with a firm physico-chemical background. Based on the developed theory, the solid diffusion coefficients of the silicon graphite (SiC) and NMC811 are determined with a commercial cell. Besides, the galvanostatic intermittent titration technique (GITT) has been applied to the same cells and the measurement results are compared with that using the DRT method. The comparison indicates that GITT cannot exclude the influence of the liquid diffusion and the solid diffusion coefficients will be underestimated.

1. Introduction

With the increasing demand for electric vehicles and renewable energy resources, the pace of technology development and manufacturing of Li-ion batteries (LIBs) is speeding up. Currently, various diagnostic methods have been used for scientific research and in practical applications. Among them the electrochemical impedance spectroscopy (EIS), as a nondestructive diagnostic method, has been used to estimate the cell states and identify the internal cell parameters. Besides the EIS measurement technology itself, measurement data evaluation and interpretation is another knotty yet important engineering problem. For LIBs, currently the equivalent circuit model (ECM) is frequently selected to fit the measured impedance data and estimate the cell parameters [1, 2]. However, the structure and the circuit components selected to build the ECM strongly rely on the experience and knowledge of the operators. Researchers are sometimes faced with the situation in which the same set of impedance data can be fitted with multiple ECMs of different structures [2]. In addition, the identifiability issue of the resulting nonlinear optimization problem may also lead to implausible results, which are simply caused by a missing comprehensive sensitivity analysis. This will sometimes result in confusing conclusions that different initial guesses lead to different solutions with the same or very close residual norm; even though a unique solution exists, it may not be easily found without using complicated optimization algorithms that are relatively computationally expensive.

1.1. Determination of the solid diffusivity with DRT

To get rid of the ambiguity of ECM fitting and resolve the identifiability issue, instead of using nonlinear optimization, the distribution of relaxation times (DRT) method has been used to deconvolve the EIS data [3–5]. For a more comprehensive modeling, the original DRT model is extended with ohmic resistance, capacitance and inductance. Moreover,

* Corresponding author.
E-mail address: yulong.zhao@tum.de (Y. Zhao).

https://doi.org/10.1016/j.electacta.2022.141174
Received 31 May 2022; Received in revised form 30 August 2022; Accepted 8 September 2022
Available online 13 September 2022

Nomenclature

Greek letters

δ	dirac delta function
κ	liquid phase conductivity, S m^{-1}
ϕ	exponent for CPE element or fractal diffusion
σ	solid phase conductivity, S m^{-1}
τ	time constant, s
θ	variable related to local particle impedance
f	frequency, Hz

Subscripts

ct	variables related to charge transfer
e	variables related to electrode or electrolyte
f	variables related to film
loc	variables related to active material particles
p	variables related to solid particles
RC	variables related to RC element
v	variables related to volume
ZARC	variables related to ZARC element

Symbols

F	Faraday constant
a	pole for meromorphic function expansion
a_v	specific volumetric area, m^{-1}
b	coefficient for meromorphic function expansion
G	DRT spectrum function of electrode
g	DRT spectrum function of RC/ZARC element
H	magnitude of dispersion peak
j	imaginary unit
l	electrode thickness, m
R	resistance (with subscript), Ω; gas constant (without subscript), J K^{-1} mol^{-1}
r	particle radius, m
s	laplace variable, jω
Y	admittance, S
Z	impedance, Ω

a comprehensive theory will be developed to explain the extended model and therefore interpret the results. The extended DRT model used in this work consists of an ohmic resistance, a series of parallel RL elements, parallel RC elements and a CPE element:

$$Z_e = R_{ohm} + \frac{1}{(j\omega C)^{\phi}} + j\omega L + \int_0^{\infty} \frac{j\omega\tau H(\tau)}{1+j\omega\tau} d\tau + \int_0^{\infty} \frac{G(\tau)}{1+j\omega\tau} d\tau \quad (1)$$

where Z_e is the measured impedance, R_{ohm} is the total ohmic resistance, $H(\tau)$ is the distribution function for the RL elements, $G(\tau)$ is the distribution function for the RC elements, C is the total capacitance and L is the total inductance. To solve the integral equation numerically, the equation above is discretized and transformed into a linear equation system. The resulting system is ill-posed by its nature and cannot be inverted directly. As a result, the regularization technique is applied to invert the equation. After discretization and transformation, the following linear optimization problem is obtained:

$$[H(\tau),\ G(\tau),\ R_{ohm},\ L,\ C] = \underset{x>0}{\operatorname{argmin}} \left\{ \| \mathbf{A}\boldsymbol{x} - \boldsymbol{b} \|_2^2 + \lambda^2 \| \mathbf{K}\boldsymbol{x} \|_2^2 \right\} \quad (2)$$

where λ is the regularization parameter, $\mathbf{A}$ is the system matrix after discretization, $\boldsymbol{b}$ is the measurement data vector, $\boldsymbol{x}$ is the solution vector, $\mathbf{K}$ is a matrix defining which variables to regularize. In this work, the distribution functions $H(\tau)$ and $G(\tau)$ are regularized.

In our previous work [6], we developed a theory to explain the DRT spectrum for the fast kinetic processes (charge transfer, SEI etc.) using a physics-based impedance model. In this work, we will try to explain the DRT spectrum for the kinetic processes with higher time constants, such as diffusion in the solid and liquid phase. Boukamp et al. [3,4] derived an analytical expression for the DRT spectrum of the finite-length-Warburg (FLW) element and investigated the performance of the resulting model. Nevertheless, the derived theory is not related to the deconvolved DRT spectrum of a LIB and does not have a comprehensive physico-chemical model behind; in addition, the derived model only considered the FLW element with transmissive boundary conditions and the capacitive behavior and other possible particle geometries are not included. Besides, no particle size distribution (PSD) is considered for the diffusion impedance. The electrode of a LIB consists of a large number of solid particles and the pores are filled with electrolyte. A complicated physico-chemical model is thus needed to describe the processes in the electrode, including the electrochemical reaction, material transport and the charge balance. Obviously, a simple equivalent circuit model with a few circuit elements cannot account for the aforementioned processes satisfactorily and the estimation results are probably problematic. Furthermore, whether and how the impedance and the resulting DRT spectra will be influenced by the aforementioned processes is still unknown. Therefore, a comprehensive theory for the DRT based on a physico-chemical model is necessary for the correct and effective estimation of the solid diffusion coefficients.

1.2. Determination of the solid diffusivity with GITT

Since proposed, the GITT has been widely applied to determine the solid diffusivity of Li-ion batteries. Due to its simple procedures, the original GITT has been used by various works to estimate the solid diffusion coefficient [7–12]. In the GITT measurement, the Li-ion battery is placed in an equilibrium state and a current pulse with a small amplitude and a duration of Δt is applied to the battery and then the battery will be fully relaxed [13]. Assuming that the overpotential caused by the dynamic processes without the ohmic conduction inside the battery is ΔE_t, the change of the equilibrium potential is ΔE_s and the diffusion length inside the solid phase is L, then the solid diffusion coefficient can be calculated as follows [13]:

$$D_{s,GITT} = \frac{4L^2}{\pi\Delta t}\left(\frac{\Delta E_s}{\Delta E_t}\right)^2 \quad (3)$$

The original GITT method applied to a Li-ion battery is based on the following assumptions: 1. the active material particles have a planar geometry; 2. all active material particles have the same size and no particle size distribution is considered; 3. the overpotential contribution caused by other dynamic processes, especially the liquid diffusion, is neglected; 4. the porous structure of the electrode and thus the transport processes inside the porous electrode are not considered. In reality, the measured overpotential in the case of a Li-ion battery is expressed by the following equation:

$$\Delta E_t = \Delta E_{t,ct} + \Delta E_{t,SEI} + \Delta E_{t,diff,l} + \Delta E_{t,diff,s} \quad (4)$$

where $\Delta E_{t,ct}$, $\Delta E_{t,SEI}$, $\Delta E_{t,diff,l}$ and $\Delta E_{t,diff,s}$ represent the overpotential attributed to the charge transfer, SEI process, liquid diffusion and solid diffusion respectively. In practical applications, the influence of the charge transfer and SEI process may be excluded if the sampling rate is high enough and an approximate time constant for the charge transfer and SEI process is assumed. However, the influence of the liquid diffusion usually cannot be effectively excluded because the diffusion time constants in the solid and liquid phases are similar. In such a case, the

Table 1
Summary and comparison of the GITT and DRT methods used for determination of the solid diffusivity.

Method	GITT		DRT	
Reference	[7–11]	[12]	[4]	Present work
Electrode model	no	no	no	physico-chemical
Particle geometry	planar	planar	planar	planar/cylindrical/spherical
Particle size distribution	no	no	no	yes
Liquid diffusion	–	excluded	–	considered
Special treatment of sample	no	yes	unknown	no

solid phase diffusivity may be underestimated if the overpotential caused by the liquid diffusion is non-negligible when compared to that caused by the solid diffusion.

To exclude the influence of the electrolytic diffusion, Kang et al. developed an improved GITT method by preparing a high-density bulk sample [12]. However, a specially prepared bulk sample with a high density was needed for the measurement so that the procedure could not be easily applied to commercial cells. Besides, the geometry and the size distribution of the particles are not considered.

1.3. Summary

From the analysis made above, it can be seen that although the DRT method can effectively separate the contribution of different processes with regard to the time constants, a comprehensive model for the interpretation of the calculated DRT spectra and thus a connection of the DRT spectra with the physico-chemical parameters are still missing. Similarly, the GITT is based on a strongly simplified case and many essential processes have been neglected.

In this work, we will try to develop a theory that can be used to interpret the DRT spectrum regarding the liquid and solid phase diffusion processes with a physics-based impedance model, a comparison of the method proposed in the present work with the existing methods is given in Table 1. Then an analytical expression for the DRT spectrum will be derived with the electrochemical parameters and the possible influence of the porous structure will be studied. With the developed DRT model based on a physico-chemical impedance model, the solid diffusion coefficient will be estimated using the DRT spectra. Meanwhile, a GITT measurement will be conducted to determine the solid diffusion coefficient, the results will be compared to that with the DRT and the advantage and effectiveness of the DRT based on a physico-chemical model will be demonstrated. The workflow of the present work is shown in Fig. 1.

The rest of the work is organized as follows: in Section 2, an analytical expression of the DRT for an electrode based on a physics-based impedance model is derived and analyzed; in Section 3, a simulation experiment will first be conducted to investigate the derived theory, then the DRT spectra of a commercial LIB and two half cells will be evaluated and interpreted using the proposed model. Section 4 concludes the work.

2. Theory development

In this section, the DRT spectra for LIBs will be investigated and an analytical expression will be developed using a physics-based impedance model. While in our previous work we have focused on the fast kinetic processes such as charge transfer and SEI process, in this work we will concentrate on the diffusion in the liquid and solid phase. The impedance model used is derived using the pseudo-two-dimensional (p2D) model developed by Doyle and Newman [14–16]. Considering that the liquid phase diffusion coefficient is usually orders of magnitude greater than that in the solid phase and that for LIBs that are not strongly aged, the liquid phase diffusivity should still be high enough, we choose to first neglect the liquid phase diffusion when investigating the solid phase diffusion, later the model will be extended by the liquid phase diffusion. The derivation of the impedance model for an electrode without liquid phase diffusion has been shown in our previous work [6] and is thus omitted here. The impedance expression is given by:

$$Z_e = \frac{l_e}{\kappa+\sigma} + \frac{(\kappa^2+\sigma^2)\coth\left(\sqrt{\theta}l_e\right)}{\kappa\sigma(\kappa+\sigma)\sqrt{\theta}} + \frac{2}{(\kappa+\sigma)\sqrt{\theta}\sinh\left(\sqrt{\theta}l_e\right)} \tag{5}$$

$$\theta = \left(\frac{1}{\sigma}+\frac{1}{\kappa}\right)\frac{1}{Z_{v,loc}} = \left(\frac{1}{\sigma}+\frac{1}{\kappa}\right)Y_{v,loc} \tag{6}$$

where Z_e is the electrode impedance, l_e is the electrode thickness, κ and σ are conductivities in the liquid and solid phases respectively, θ is a variable related to the local particle impedance and $Z_{v,loc}$ and $Y_{v,loc}$ are the volume-specific particle impedance and admittance respectively. The volume-specific impedance instead of the area-specific impedance is used to ease the derivation for the case where the PSD is considered.

2.1. Classification of dispersion phenomena in electrodes

According to our previous work [6], the porous structure and transport phenomena in the electrode will cause dispersion behavior with regard to the charge transfer and SEI processes when the diffusion is neglected in the mid-high frequency range. In the low frequency range where the diffusion cannot be neglected, it is still unclear whether the spectra will be influenced by the dispersion and how pronounced it will be. Hence, we start by analyzing the dispersion phenomenon in the low frequency range. We believe that according to the electrochemical processes occurring in an electrode, the spectrum dispersion has two origins: the first kind of dispersion is caused by the spatially distributed physical or electrochemical processes along the thickness of the electrode, such as the electronic/ionic conduction and the distributed electrochemical reactions, we refer to the first kind of dispersion as stage one dispersion. Another kind of dispersion arises from the local

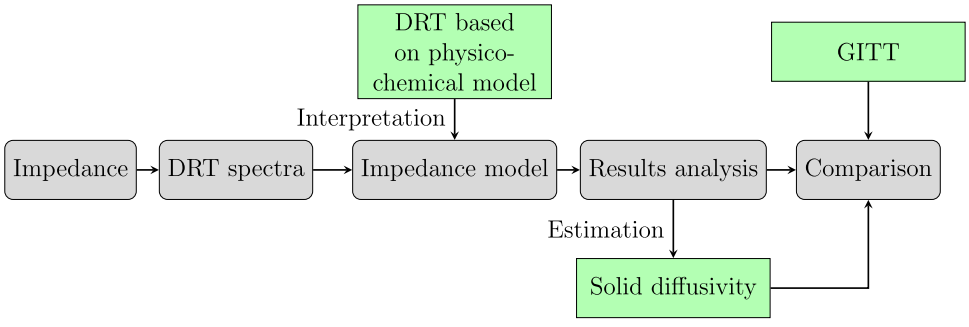

Fig. 1. Workflow of determination of the solid diffusion coefficient using DRT and a physicochemical impedance model.

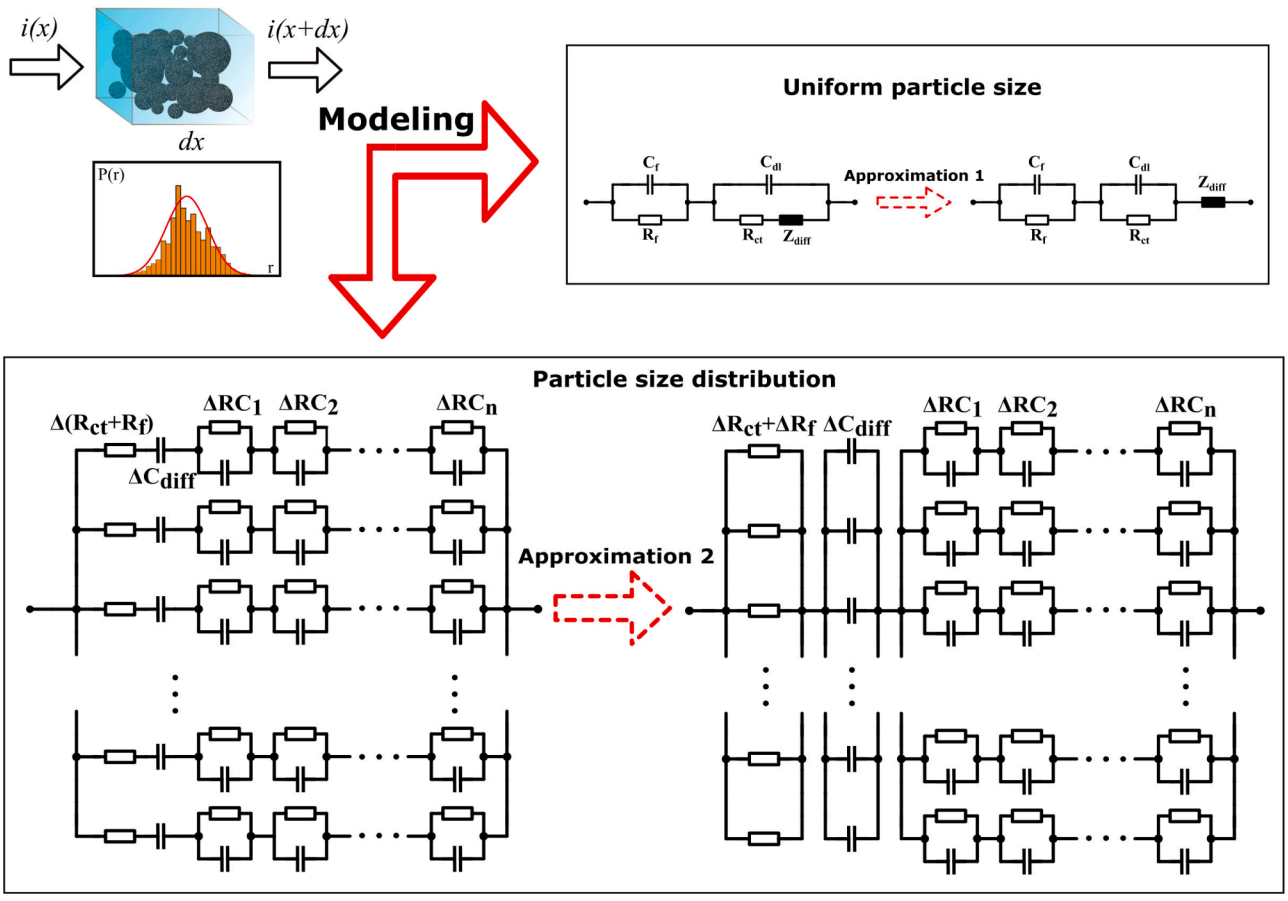

Fig. 2. Circuit approximation used for the model development, with approximation 1 in the upper part and approximation 2 in the lower part of the figure.

processes which will locally cause dispersion itself, such as charge transfer with a constant phase element (CPE) and the solid phase diffusion. We refer to the second kind of dispersion as stage two dispersion. Both dispersion behaviors are not simply linearly superimposed but rather interacting with each other in a sophisticated way, a direct investigation of all dispersion phenomena at the same time will lead to an overly complicated mathematical problem which does not help to resolve the issue. Based on the cause and the scope of impact of the dispersion phenomena, we choose to develop the theory with a two-step procedure by investigating the dispersion of two stages separately. In the following sections, we will conduct the model derivation starting from stage one dispersion. Then, the stage two dispersion will be investigated based on the findings and conclusions from the stage one dispersion.

2.2. Stage one dispersion: electrode level dispersion

In this section the stage one dispersion phenomenon will be investigated. Upon substituting Eq. (6) into (5), a meromorphic function of the volume-specific admittance $Y_{v,loc}$ is obtained, which can be reformulated as an infinite series using the Mittag–Leffler theorem [17]:

$$Z_e = Z_{e,Y_{v,loc,0}} + \sum_{n=0}^{\infty}\left(\frac{B_n}{Y_{v,loc} - A_n} + \frac{B_n}{A_n}\right) \tag{7}$$

where A_n and B_n are the corresponding poles and expansion coefficients respectively, $Z_{e,Y_{v,loc,0}}$ is the electrode impedance when $Y_{v,loc}$ approaches zero. If we let $Y_{v,loc}$ approach infinity (equivalent to $f \to \infty$) and evaluate the resulting equation, the following equation can be obtained:

$$Z_{e,Y_{v,loc,0}} + \sum_{n=0}^{\infty}\frac{B_n}{A_n} = \frac{l_e}{\kappa + \sigma} \tag{8}$$

The equation above is substituted into Eq. (7) and the following simplified equation is obtained:

$$Z_e = \frac{l_e}{\kappa + \sigma} + \sum_{n=0}^{\infty}\left(\frac{B_n}{Y_{v,loc} - A_n}\right) \tag{9}$$

In the equation derived above, $l_e/(\kappa+\sigma)$ is the ohmic resistance of the electrode. The poles of the expansion are determined by solving the following equations:

$$\theta = 0 \quad (n = 0) \tag{10}$$

$$\sinh\left(\sqrt{\theta_n} l_e\right) = 0 \Rightarrow \sqrt{\theta_n} l_e = in\pi \quad (n = 1, 2, 3, \ldots) \tag{11}$$

The solutions to the equations above are given as:

$$A_0 = 0 \quad (n = 0) \tag{12}$$

$$A_n = -\frac{n^2\pi^2}{l_e^2\left(\frac{1}{\kappa} + \frac{1}{\sigma}\right)} \quad (n = 1, 2, 3, \ldots) \tag{13}$$

And the expansion coefficients B_n are solved for using the residue method:

$$B_n = \lim_{Y_{v,loc} \to A_n}\left(Y_{v,loc} - A_n\right) Z_e\left(Y_{v,loc}\right) \tag{14}$$

which gives the following solutions:

$$B_0 = \frac{1}{l_e} \tag{15}$$

Table 2
Solid diffusion impedance with different geometric shapes [18].

Particle geometry	Planar	Cylindrical	Spherical
Z_d	$\frac{\coth(\sqrt{s\tau_0})}{\sqrt{s\tau_0}}$	$\frac{I_0(\sqrt{s\tau_0})}{\sqrt{s\tau_0}I_1(\sqrt{s\tau_0})}$	$\frac{\tanh(\sqrt{s\tau_0})}{\sqrt{s\tau_0}-\tanh(\sqrt{s\tau_0})}$
R_d		$\left(-\frac{\partial U}{\partial c_s}\right)\frac{r_p}{FD_s}$	

$$B_n = \frac{2[\kappa^2 + 2\kappa\sigma(-1)^n + \sigma^2]}{l_e(\kappa+\sigma)^2} \quad (n = 1, 2, 3, \ldots) \tag{16}$$

It can be seen from Eqs. (13) to (16) that the poles are a function of n and increase with the factor n^2, the expansion coefficients are swinging between two constant values and thus not decaying with increasing order. A qualitative inspection of Eqs. (9), (13) and (16) indicates that even the expansion coefficients are not decaying with increasing order, the denominator increases with increasing n because the poles are increasing. Through further model investigation, we can confirm that the dispersion magnitude decays quickly with the increasing time constants, so that for the solid diffusion process the stage one dispersion can be practically neglected. In order to show quantitatively that the magnitude of dispersion terms decreases with increasing time constants, the theorem on residue of composition function can be used to derive the coefficients corresponding to each process, the derivation is provided in Appendix A.4.

2.3. Stage two dispersion: particle dispersion

In the last section, we have analyzed the stage one dispersion in detail and concluded that the stage one dispersion can be practically neglected in the low frequency range. In this section, we will continue to investigate the local dispersion phenomena.

The area-specific local particle impedance of a LIB is usually expressed using the following equation [2]:

$$Z_{loc} = \frac{R_f}{1+sR_fC_f} + \frac{1}{\frac{1}{R_{ct}+R_dZ_d}+sC_{dl}} \tag{17}$$

where R_f and R_{ct} are the film and charge transfer resistances respectively, C_f and C_{dl} are the film and double layer capacitances respectively, Z_d is the dimensionless diffusion impedance and R_d represents the diffusional resistance. For brevity, here we have only considered RC elements for charge transfer and SEI process, for ZARC elements a similar model can be derived, as shown in our previous work [6].

Due to the fact that the diffusion time constants are usually several orders of magnitude larger than those of the charge transfer and SEI processes, the particle impedance can be approximated with a series connection of two RC elements and one diffusion impedance (see Fig. 2):

$$Z_{loc} \approx \frac{R_f}{1+sR_fC_f} + \frac{R_{ct}}{1+sR_{ct}C_{dl}} + R_dZ_d \tag{18}$$

We refer to the approximation made above as approximation 1. Depending on the geometric shape of the particles, the dimensionless diffusion impedance Z_d has different forms which are listed in Table 2, where U is the open circuit voltage of the electrode, r_p is the particle size, c_s is the concentration of the Li-ions in the particles, τ_0 is the characteristic diffusion time constant with $\tau_0 = r_p^2/D_s$. An electrode with a uniform particle size (UPS) is only a strongly simplified case. In reality, the active material particles inside the electrode have a particular PSD, which will modify the diffusion impedance of a LIB in a specific way. In the following sections, the dispersion phenomenon as well as the DRT spectrum for the solid diffusion will be discussed in two cases: solid particles with UPS and PSD.

Table 3
Expansion parameters of diffusion impedance (see Appendices A.1–A.3).

Geometry	τ_n	R_n	C_d	λ_n
Planar	$\frac{\tau_0}{\lambda_n^2}$	$\frac{2}{\lambda_n^2}$	τ_0	$n\pi$
Cylindrical	$\frac{\tau_0}{\lambda_n^2}$	$\frac{2}{\lambda_n^2}$	$\frac{\tau_0}{2}$	$J_1(\lambda_n) = 0$
Spherical	$\frac{\tau_0}{\lambda_n^2}$	$\frac{2}{\lambda_n^2}$	$\frac{\tau_0}{3}$	$\tan(\lambda_n) = \lambda_n$

2.3.1. Diffusion with uniform particle size

If the solid particles have a uniform size, the volume-specific particle impedance can be obtained by simply scaling the area-specific impedance using the volumetric interfacial area a_v:

$$Z_{v,loc} = \frac{Z_{loc}}{a_v} = \frac{1}{a_v}\left(\frac{R_f}{1+sR_fC_f} + \frac{R_{ct}}{1+sR_{ct}C_{dl}}\right) + \frac{1}{a_v}R_dZ_d \tag{19}$$

If we first neglect the higher order dispersion terms and only keep the 0th order terms, Eq. (9) can be rewritten as:

$$Z_{e,0} = \underbrace{\frac{l_e}{\kappa+\sigma}}_{\text{Ohmic resistance}} + \underbrace{\frac{1}{a_vl_e}\left(\frac{R_f}{1+sR_fC_f} + \frac{R_{ct}}{1+sR_{ct}C_{dl}}\right)}_{\text{Charge transfer and SEI process}} + \underbrace{\frac{1}{a_vl_e}R_dZ_d}_{\text{Solid diffusion}} \tag{20}$$

The resulting expression is equivalent to the well-known single particle model (SPM) assumption [19] and has a clear physical meaning: the first term represents the ohmic resistance of the electrode, the second term represents the charge transfer and SEI impedance, the last term is the diffusion impedance in the solid phase. The approximated electrode impedance represented by the equation above assumes that the higher order stage one dispersion is neglected, which is only true in the low frequency range. For processes with smaller time constants, a certain dispersion is expected and will cause discrepancy when compared to the original impedance. The dispersion phenomena in the mid-high frequency range has been studied in detail in our previous work. An alternative way to approximate the total electrode impedance is given as:

$$Z_{e,appr} = Z_{hf} + \frac{1}{a_vl_e}R_dZ_d \tag{21}$$

where Z_{hf} is the electrode impedance in the mid-high frequency range, in which the solid phase diffusion is neglected:

$$Z_{hf} = \frac{l_e}{\kappa+\sigma} + \frac{(\kappa^2+\sigma^2)\coth\left(\sqrt{\theta_{hf}}l_e\right)}{\kappa\sigma(\kappa+\sigma)\sqrt{\theta_{hf}}} + \frac{2}{(\kappa+\sigma)\sqrt{\theta_{hf}}\sinh\left(\sqrt{\theta_{hf}}l_e\right)} \tag{22}$$

$$\theta_{hf} = \left(\frac{1}{\sigma}+\frac{1}{\kappa}\right)\left(\frac{R_f}{1+sR_fC_f} + \frac{R_{ct}}{1+sR_{ct}C_{dl}}\right)^{-1} \tag{23}$$

In order to show the discrepancy caused by the dispersion in the mid-high frequency range, we still choose Eq. (20) to reconstruct the impedance and compare the results. Next, to characterize the dispersion caused by the local solid diffusion in the particles, the dimensionless diffusion impedance Z_d is expanded as a sum of a capacitance and an infinite number of serially connected RC elements using the Mittag–Leffler theorem:

$$Z_d = \frac{1}{sC_d} + \sum_{n=1}^{\infty}\frac{R_n}{1+s\tau_n} \tag{24}$$

The expansion coefficients and dispersion time constants for particles of different geometries are listed in Table 3 and the detailed derivation can be found in Appendices A.1–A.3. When conducting the DRT analysis, the ohmic resistance, inductive and capacitive components as well as the DRT spectrum will be calculated by an optimization algorithm. By combining Eqs. (20) and (24) and considering Table 3, the DRT spectrum can be expressed using the following equation:

$$G(\tau)=\frac{1}{a_v l_e}\left[R_{ct}\delta(\tau-\tau_{ct})+R_f\delta(\tau-\tau_f)\right]+\sum_{n=1}^{\infty}\left(-\frac{\partial U}{\partial c_s}\right)\frac{r_p R_n}{a_v l_e F D_s}\delta(\tau-\tau_n) \tag{25}$$

We further notice that $a_v=N\epsilon_s/r_p$ and $C_d=\tau_0/N$, where N is the particle geometry index and $N=1,2,3$ stands for planar, cylindrical and spherical particles respectively. The total electrode capacitance is given by:

$$C_e=\frac{\epsilon_e l_e F}{\left(-\frac{\partial U}{\partial c_s}\right)} \tag{26}$$

Eq. (25) implies that the DRT spectrum corresponding to the solid phase diffusion consists of an infinite sum of Dirac delta functions with decreasing magnitude and time constants. We further notice that $\lambda_n\approx n\pi$ regardless of the particle geometry. Therefore both the dispersion time constants and magnitudes also decay approximately with the factor $1/n^2$. By conducting DRT analysis, the diffusion time constants as well as the diffusion coefficients can be estimated using the relation listed in Table 3 if the particle geometry and size are known. Eq. (26) indicates that the capacitance of the electrode is decided by the electrode thickness l_e, volume fraction of active material ϵ_s and the differential open circuit voltage (dOCV). The magnitude of the prominent peak (peak with the largest magnitude and time constants) can be calculated as:

$$H_1=\left(-\frac{\partial U}{\partial c_s}\right)\frac{2\tau_1}{3\epsilon_s l_e F} \tag{27}$$

2.3.2. Diffusion with particle size distribution

In this section, the DRT spectrum for an electrode with a PSD will be derived and investigated. In practice, the particles in the electrode have a certain size distribution, which has a significant influence on the diffusion part of the impedance curve and cannot be neglected [20]. In this work, we will try to approximate the analytical DRT spectrum when the PSD is taken into account. Based on the theoretical investigation, an approximation method is proposed to interpret the DRT spectrum when considering the PSD. As in many practical applications of the p2D model the solid particles are assumed to be spherical [14–16], thus we choose to derive the model with spherical particle geometry. For particles with a planar or cylindrical geometry, the same development procedures can be performed and similar conclusions can be made.

In an infinitesimally small volume element, in which the potential in the liquid and solid phases can be regarded as spatially constant, the volume-specific particle impedance can be defined as:

$$Z_{v,loc}=\frac{\Phi_s-\Phi_l}{i_{v,loc}} \tag{28}$$

where Φ_s and Φ_l are potentials in the solid and liquid phases respectively, $i_{v,loc}$ is the local volumetric reaction current density. Using the PSD, the volumetric current density can be expressed as:

$$i_{v,loc}=\int_0^{\infty}4\pi r^2 N(r)i_{loc}(r)dr=\int_0^{\infty}4\pi r^2 N(r)\frac{\Phi_s-\Phi_l}{Z_{loc}(r)}dr \tag{29}$$

where r is the particle radius, $N(r)$ is the PSD function inside the unit volume and i_{loc} is the local area-specific reaction current density. Upon substituting Eq. (29) into (28), the volumetric particle impedance can be formulated as:

$$Z_{v,loc}=\frac{\Phi_s-\Phi_l}{i_{v,loc}}=\left[\int_0^{\infty}\frac{4\pi r^2 N(r)}{Z_{loc}(r)}dr\right]^{-1} \tag{30}$$

To simplify the model derivation and enable an explicit expression, the following assumptions are made:

1. The ohmic resistance, capacitance and RC elements contribution to the local impedance can be approximately separated, to which we refer as as approximation 2, as depicted in Fig. 2.
2. Because the magnitude of the solid diffusion impedance dispersion decreases with $1/n^2$ (see Table 3), the main component of the diffusion impedance can be approximated by the the first three RC elements with the largest three time constants ($\sum_{n=1}^{3}1/\lambda_n^2\approx 0.75\sum_{n=1}^{\infty}1/\lambda_n^2$), to which we refer as the 3RC approximation.

Due to the fact that the diffusion mainly occurs in the low frequency range ($f\ll 1$ Hz), we neglect the terms $s^n\quad(n\geq 1)$ in the nominator and $s^n\quad(n\geq 2)$ in the denominator when summing the three RC elements up. Note that the resistances and time constants are related by λ_n (see Table 3), the following approximated expression is obtained:

$$Z_{3RC}=\sum_{n=1}^{n=3}\frac{R_n}{1+s\tau_n}\approx\frac{R_{3RC}}{1+s\tau_{3RC}} \tag{31}$$

where the corresponding resistance and time constant are given as:

$$R_{3RC}=\left(1+\frac{\lambda_1^2\lambda_2^2+\lambda_1^2\lambda_3^2}{\lambda_2^2\lambda_3^2}\right)R_1=\mu R_1 \tag{32}$$

$$\tau_{3RC}=\left(1+\frac{\lambda_1^2\lambda_2^2+\lambda_1^2\lambda_3^2}{\lambda_2^2\lambda_3^2}\right)\tau_1=\mu\tau_1 \tag{33}$$

It can be seen that the approximated resistance and time constant are both scaled with the same factor μ which is larger than one. With the assumptions and approximations made above, Eq. (30) can be reformulated as:

$$Z_{v,loc}=\left[\int_0^{\infty}\frac{4\pi r^2 N(r)}{\frac{R_f}{1+sR_fC_f}+\frac{R_{ct}}{1+sR_{ct}C_{dl}}}dr\right]^{-1}+\left[s\int_0^{\infty}4\pi r^2 N(r)\frac{rF}{3\left(-\frac{\partial U}{\partial c_s}\right)}dr\right]^{-1}+\left[\frac{FD_s\lambda_1^2}{\mu\left(-\frac{\partial U}{\partial c_s}\right)}\int_0^{\infty}2\pi rN(r)dr+\frac{sF}{\left(-\frac{\partial U}{\partial c_s}\right)}\int_0^{\infty}2\pi r^3N(r)dr\right]^{-1} \tag{34}$$

Note that the following relations hold for the PSD:

$$a_v=\int_0^{\infty}4\pi r^2N(r)dr \tag{35}$$

$$\epsilon_s=\int_0^{\infty}\frac{4}{3}\pi r^3N(r)dr \tag{36}$$

$$\overline{r_p}=\frac{\int_0^{\infty}rN(r)dr}{N_p}=\int_0^{\infty}rP(r)dr \tag{37}$$

where a_v is the volumetric interfacial area defined by the PSD, $\overline{r_p}$ is the average particle radius, N_p is the total number of the solid particles in unit volume, $P(r)$ is the probability density function (PDF) of the particle radius. N_p and $P(r)$ are defined as:

$$N_p=\int_0^{\infty}N(r)dr \tag{38}$$

$$P(r)=\frac{N(r)}{N_p} \tag{39}$$

If we substitute Eqs. (35)–(39) into Eq. (34), the following equation is obtained:

$$Z_{\mathrm{v,loc,3RC}} = \frac{1}{a_\mathrm{v}}\left(\frac{R_\mathrm{f}}{1+sR_\mathrm{f}C_\mathrm{f}} + \frac{R_\mathrm{ct}}{1+sR_\mathrm{ct}C_\mathrm{dl}}\right) + \frac{1}{s\frac{\mathrm{F}\epsilon_\mathrm{s}}{\left(-\frac{\partial U}{\partial c_\mathrm{s}}\right)}} + \left[\frac{2\pi\mathrm{F}D_\mathrm{s}\lambda_1^2 N_\mathrm{p}\overline{r_\mathrm{p}}}{\mu\left(-\frac{\partial U}{\partial c_\mathrm{s}}\right)} + s\frac{3\mathrm{F}\epsilon_\mathrm{s}}{2\left(-\frac{\partial U}{\partial c_\mathrm{s}}\right)}\right]^{-1} \tag{40}$$

After the approximated local volume-specific particle impedance has been derived, the impedance must be scaled to obtain the electrode impedance. In Section 2.2, the electrode impedance expression has been expanded with regard to $Y_{\mathrm{v,loc}}$. Similarly, the dispersion terms are neglected here due to the reasons explained before, the final expression for the approximated electrode impedance is given as:

$$Z_\mathrm{e} = \frac{l_\mathrm{e}}{\kappa+\sigma} + \frac{1}{a_\mathrm{v}l_\mathrm{e}}\left(\frac{R_\mathrm{f}}{1+sR_\mathrm{f}C_\mathrm{f}} + \frac{R_\mathrm{ct}}{1+sR_\mathrm{ct}C_\mathrm{dl}}\right) + \frac{1}{s\frac{\mathrm{F}l_\mathrm{e}\epsilon_\mathrm{s}}{\left(-\frac{\partial U}{\partial c_\mathrm{s}}\right)}} + \left[\frac{2\pi l_\mathrm{e}\mathrm{F}D_\mathrm{s}\lambda_1^2 N_\mathrm{p}\overline{r_\mathrm{p}}}{\mu\left(-\frac{\partial U}{\partial c_\mathrm{s}}\right)} + s\frac{3l_\mathrm{e}\mathrm{F}\epsilon_\mathrm{s}}{2\left(-\frac{\partial U}{\partial c_\mathrm{s}}\right)}\right]^{-1} \tag{41}$$

The equation above has a clear physical meaning and can be readily interpreted as follows:

1. The first term is the ohmic resistance of the electrode.
2. The second term represents the charge transfer and SEI impedance, which is simply the scaled local particle impedance and is equivalent to the SPM. As explained before, the first and second term can also be replaced by the electrode impedance without solid diffusion (see Eqs. (22) and (23)) to account for the dispersion terms in the mid-high frequency range:

$$Z_\mathrm{e} = Z_\mathrm{hf} + \frac{1}{s\frac{\mathrm{F}l_\mathrm{e}\epsilon_\mathrm{s}}{\left(-\frac{\partial U}{\partial c_\mathrm{s}}\right)}} + \left[\frac{2\pi l_\mathrm{e}\mathrm{F}D_\mathrm{s}\lambda_1^2 N_\mathrm{p}\overline{r_\mathrm{p}}}{\mu\left(-\frac{\partial U}{\partial c_\mathrm{s}}\right)} + s\frac{3l_\mathrm{e}\mathrm{F}\epsilon_\mathrm{s}}{2\left(-\frac{\partial U}{\partial c_\mathrm{s}}\right)}\right]^{-1} \tag{42}$$

3. The third term represents the approximated total electrode capacitance when the PSD is also taken into consideration. We can also observe that the total electrode capacitance has the same form as that of UPS and is thus not dependent on the PSD (see Eq. (26)).
4. The last term represents an RC element arising from the solid diffusion with the PSD and can be used to estimate the diffusion parameters.

The time constant of the RC element for the solid diffusion with the PSD defined above is given as:

$$\tau_\mathrm{PSD} = \frac{3\mu\epsilon_\mathrm{s}}{4\pi D_\mathrm{s}N_\mathrm{p}\lambda_1^2\overline{r_\mathrm{p}}} \tag{43}$$

Similarly, the magnitude of the prominent peak is given as:

$$H_{1,\mathrm{3RC}} = \frac{\mu\left(-\frac{\partial U}{\partial c_\mathrm{s}}\right)}{2\pi l_\mathrm{e}\mathrm{F}D_\mathrm{s}\lambda_1^2 N_\mathrm{p}\overline{r_\mathrm{p}}} \tag{44}$$

The equations derived above indicate that although with the DRT spectrum the exact PSD cannot be determined in a straightforward way, still it can reflect particular average quantities of the electrode and can be used to estimate the diffusivity if specific electrode parameters are given. Furthermore, Eq. (43) also indicates that the time constant, when the PSD is considered, cannot be simply calculated using $\overline{r_\mathrm{p}}^2/D_\mathrm{s}\lambda_1^2$, which will underestimate the diffusion time constant, especially when the PSD has a relatively high variance. Again the approximation and analysis made above assume that the higher order terms of the stage one dispersion are neglected. For the high frequency processes, the dispersion generally cannot be neglected.

2.4. Fractal diffusion

In practical applications, it is often found that in the low frequency area, instead of an ideal capacitive impedance ($|\theta| = 90°$), a CPE-type impedance ($|\theta| < 90°$) is observed. Correspondingly, in the Warburg region, slightly depressed circles are expected. The existence of such non-ideal diffusion behavior is usually attributed to the nonuniform diffusion or multiple paths in the system [1]. As a result, the $(s\tau_0)$ term in Table 2 is replaced by $(s\tau_0)^\phi$, where ϕ is the parameter describing the fractal diffusion and $\phi \leq 1$. When the fractal diffusion behavior is expected, the characterization method must be adapted to correctly estimate the parameters. Eq. (1) Then the time constants read from the DRT spectrum are related to the diffusion coefficients through the following equation:

$$\left(\frac{\tau_0}{\tau_n}\right)^\phi = \lambda_n^2 \tag{45}$$

As a prerequisite, the parameter ϕ must first be estimated with the capacitive impedance of the EIS.

2.5. Diffusion in the electrolyte

When the diffusivity in the electrolyte is large enough so that the electrolytic diffusion is no more a limiting factor, the impedance contribution of electrolytic diffusion can be practically neglected. In most published works related to DRT, the electrolytic diffusion is simply neglected, which may potentially cause errors when the assumption made above is not fulfilled [5,18,21,22]. Zhou et al. investigated a LIB using the DRT and emphasized the importance of considering the electrolytic diffusion [23]. However, an investigation of the qualitative and quantitative relation between the impedance and the DRT spectrum was not provided. Therefore, in this work we will propose an extended model to account for the electrolytic diffusion in a simplified way, based on which the DRT spectrum will be interpreted and explained.

To develop the model which can be used to derive the DRT expressions for the electrolytic diffusion, an analytical solution is a prerequisite. Sikha et al. developed an analytical solution for the impedance of a LIB and managed to simulate the cell impedance with physicochemical parameters [24,25]. Despite the closed-form solution, it cannot be directly used to derive the DRT expression due to its complicated form. Here we try to separate the contribution of electrolytic diffusion from the total impedance. We assume that the reaction current density is homogeneous along the electrode thickness, thus the equation for the Li-ion transport in the electrolyte is decoupled and can be rewritten as follows:

$$s\epsilon_\mathrm{e}\widetilde{c}_\mathrm{e} = \frac{\partial}{\partial x}\left(D_\mathrm{e,eff}\frac{\partial\widetilde{c}_\mathrm{e}}{\partial x}\right) + \frac{a_\mathrm{v}\widetilde{j}_\mathrm{loc}(1-t_+)}{\mathrm{F}} \tag{46}$$

where $\widetilde{c}_\mathrm{e}$ is the liquid phase concentration, $D_\mathrm{e,eff}$ is the effective liquid phase diffusivity, s is the laplace variable and $s = j\omega$, $\widetilde{j}_\mathrm{loc}$ is the local reaction current density and is related to the total applied current density $\widetilde{i}_\mathrm{app}$ by:

$$\widetilde{j}_\mathrm{loc} = \frac{\widetilde{i}_\mathrm{app}}{a_\mathrm{v}l_\mathrm{e}} \tag{47}$$

The equation derived above is subjected to the following boundary conditions:

$$D_\mathrm{e,eff}\frac{\partial\widetilde{c}_\mathrm{e}}{\partial x}\Big|_{x=0} = 0 \tag{48}$$

$$\widetilde{c}_\mathrm{e}|_{x=l_\mathrm{e}} = 0 \tag{49}$$

Table 4
Summary of time constants for diffusion in the solid and liquid phases.

Physics	Solid diffusion		Liquid diffusion
Particle size	UPS	PSD	-
Time constant	$\frac{r_p^2}{D_s\lambda_1^2}$	$\frac{3\mu\epsilon_s}{4\pi D_s N_p \lambda_1^2 \overline{r_p}}$	$\frac{4\epsilon_l l_e^2}{\pi^2 D_{e,\text{eff}}}$
Approximation	1	1,2,3RC	SPM

Eq. (46) can be easily solved to obtain the following solution:

$$\widetilde{c}_e(x=0) = \widetilde{i}_{app}\frac{1-t_+}{F\epsilon_l l_e}\left(\frac{1}{s} - \frac{1}{s\cosh\left(\sqrt{s\tau_{l,0}}\right)}\right) \tag{50}$$

where $\tau_{l,0}$ is the characteristic diffusion time in the electrolyte and is defined as follows:

$$\tau_{l,0} = \epsilon_l \frac{l_e^2}{D_{l,\text{eff}}} \tag{51}$$

The overpotential caused by the electrolytic diffusion in the LIB is defined as:

$$\eta_{l,\text{diff}} = \frac{2RT(1-t_+)}{Fc_{l,0}}\left(1+\frac{\partial \ln\gamma}{\partial \ln c}\right)\Delta c_l \tag{52}$$

Note that the impedance caused by the electrolytic diffusion is:

$$Z_{l,\text{diff}} = \frac{\eta_{l,\text{diff}}}{\widetilde{i}_{app}} \tag{53}$$

As a result, the electrolytic diffusion impedance can be expressed:

$$Z_{l,\text{diff}} = \frac{2RT(1-t_+)^2}{F^2\epsilon_l l_e c_{l,0}}\left(1+\frac{\partial \ln\gamma}{\partial \ln c}\right)\left(\frac{1}{s} - \frac{1}{s\cosh\left(\sqrt{s\tau_{l,0}}\right)}\right) \tag{54}$$

By applying the Mittag–Leffler theorem to the impedance expression, a series can be obtained:

$$Z_{l,\text{diff}} = \sum_{i=0}^{+\infty}\frac{b_n}{s-a_n} \tag{55}$$

where the expansion poles and coefficients are defined as follows:

$$a_n = -\frac{\pi^2\left(n+\frac{1}{2}\right)^2}{\tau_{l,0}} \tag{56}$$

$$b_n = \frac{4(-1)^n(1-t_+)^2RT}{(2n+1)\pi F^2\epsilon_l l_e c_{l,0}}\left(1+\frac{\partial \ln\gamma}{\partial \ln c}\right) \tag{57}$$

The equations derived above indicate that the contribution of the electrolytic diffusion corresponds to a series of peaks in the DRT spectrum with decreasing magnitude and time constants. But as the dispersion terms decay very fast, usually only one peak can be observed. The time constant $\tau_{l,n}$ and magnitude h_n of each peak is calculated as:

$$\tau_{l,n} = -\frac{1}{a_n} = \frac{\tau_{l,0}}{\pi^2\left(n+\frac{1}{2}\right)^2} \tag{58}$$

$$h_n = -\frac{b_n}{a_n} = \frac{32(-1)^n(1-t_+)RT\tau_{l,0}}{(2n+1)^3\pi^3F^2\epsilon_l l_e c_{l,0}}\left(1+\frac{\partial \ln\gamma}{\partial \ln c}\right) \tag{59}$$

Because the fundamental order peak has the largest magnitude and can be better observed, the time constant of the fundamental order peak can be used to estimate the effective diffusivity in the electrolyte.

2.6. Summary of model and theory

In the previous sections, we have investigated the DRT spectrum of the LIB and the characterization of diffusion in the solid and liquid phases. For the case of UPS, given the particle radius, the solid phase diffusivity can be simply estimated by reading the time constants from the DRT spectrum. When the particle size is nonuniform and has a certain PSD, more information about the PSD is needed to estimate the diffusivity more accurately. In addition, to account for the diffusion in the liquid phase, an extended model is proposed to estimate the effective diffusivity in the liquid phase, the diffusivity can be estimated with the DRT spectrum, if the electrode thickness and porosity are known. For briefness, the proposed models and conclusions are summarized in Table 4.

Table 5
Parameters used for simulation experiments.

Electrode	Anode	Separator	Cathode
Design and geometric parameters			
Electrode thickness l_e [μm]	86.7[c]	12[c]	66.2[c]
Active material volume fraction ϵ_s [%]	69.4[c]	–	74.5[c]
Porosity ϵ_l [%]	21.6[c]	45[c]	17.1[c]
Bruggeman coefficient α [–]	1.5[c]	1.5[c]	1.85[c]
Transport parameters			
Ionic conductivity κ [m S^{-1}]	0.1199[bdg]	0.3605[bdg]	0.0455[bdg]
Electronic conductivity σ [m S^{-1}]	57.81[bdg]	–	0.0986[bdg]
Solid diffusivity D_s [$\text{m}^2\ \text{s}^{-1}$]	1×10^{-13}[a]	–	5×10^{-15}[a]
Liquid diffusivity D_l [$\text{m}^2\ \text{s}^{-1}$]	6.47×10^{-11}[a]	1.94×10^{-10}[a]	2.46×10^{-11}[a]
Thermodynamic parameters			
Differential OCV $\frac{\partial U}{\partial c_s}$ [$\text{Vm}^{-3}\ \text{mol}^{-1}$]	Calculated with the data from [26]		
Kinetic parameters			
Reaction rate constant k [ms^{-1}]	3×10^{-11}[c]	–	1×10^{-11}[c]
Film resistance R_f [Ωm^2]	0.0035[c]	–	0[c]
Double layer capacitance C_{dl} [Fm^{-2}]	0.2[a]	–	1[a]
Film capacitance C_f [Fm^{-2}]	0.1[a]	–	–
Simulation parameters			
Frequency f [Hz]	$5\times10^{-3}\sim10^4$		
Number of frequency points N_f	70 (logarithmic)		

[a] assumed.
[b] calculated.
[c] Ref. [26].
[d] Ref. [27].
[g] bulk value from literature and effective value calculated using Bruggeman relation.

Table 6
Summary of the particle size distribution parameters.

Electrode	Anode			Cathode		
Model	UPS	PSD		UPS	PSD	
Case	A	B	C	A	B	C
$r_{p,D50}$ [μm]	6.1	6.1	6.1	3.8	3.8	3.8
$\overline{r_p}$ [μm]	6.1	6.03	6.5	3.8	3.76	4.0
r_{min} [μm]	–	0.1	0.1	–	0.1	0.1
N_p [–]	7.3×10^{14}	6.6×10^{14}	3.2×10^{14}	3.2×10^{15}	3.0×10^{15}	1.4×10^{15}
a [–]	–	6.5×10^{-6}	7.2×10^{-6}	–	4.0×10^{-6}	4.4×10^{-6}
b [–]	–	5	2	–	5	2

3. Results and discussion

In this section, the proposed theory is first investigated and validated using synthetic simulation experiments, where the developed model will be tested in various cases. Then the theory will be applied to a commercial cell, the impedance and DRT spectra will be analyzed and the

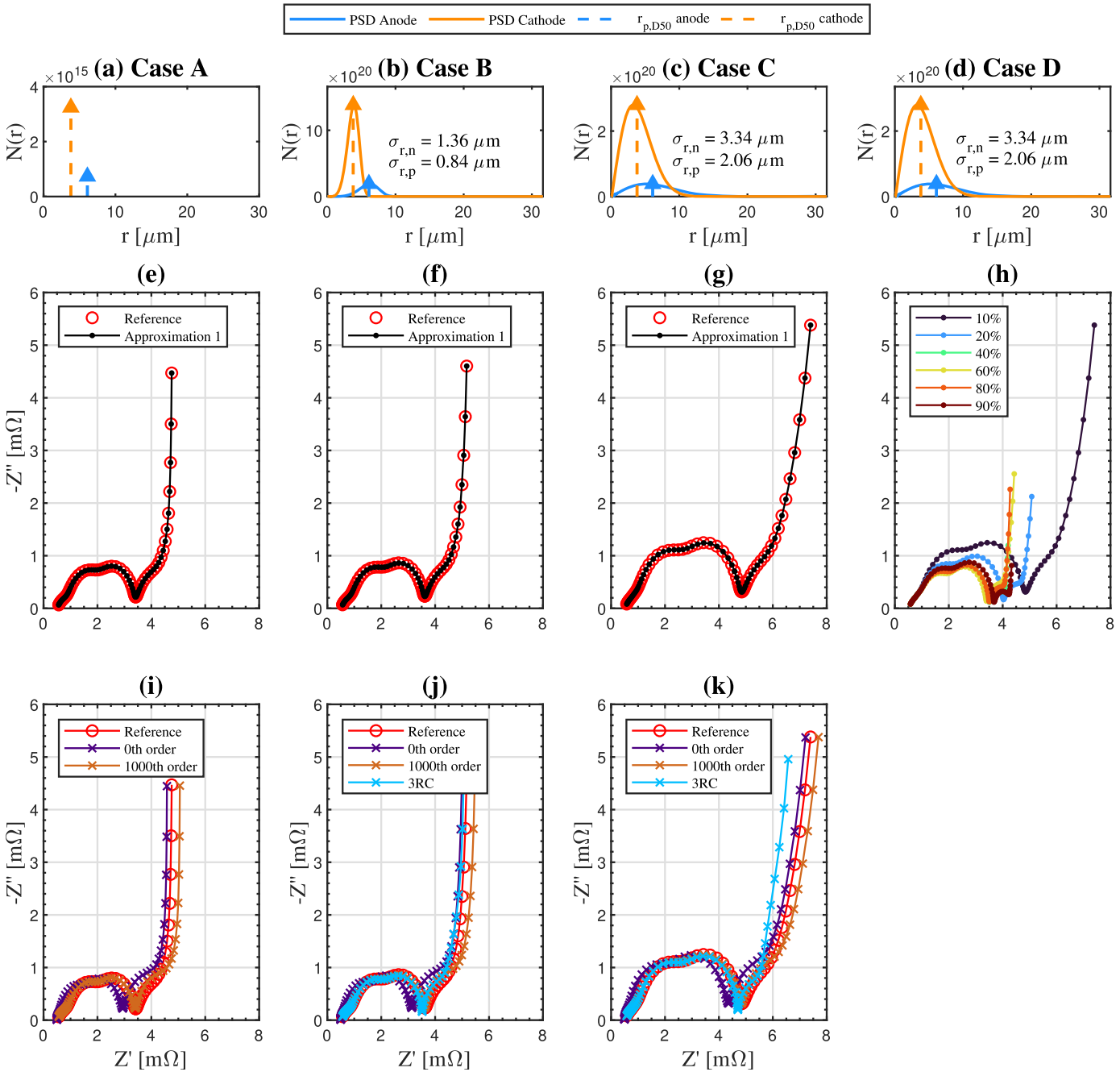

Fig. 3. Comparison of original model and the model with approximation 1. (a)–(d): the PSD used for the simulation; (e)–(g): comparison of the reference impedance with impedance generated using assumption one; (i)–(k): reconstructed impedance using different orders; (h): generated impedance at different SOCs.

diffusion coefficients will be estimated (Table 6).

3.1. Synthetic simulation experiments

In this section, a synthetic simulation experiment will be conducted to validate the proposed theory and a detailed analysis of the results will be provided. To compare the results with regard to the PSD and show the effectiveness of the model when the PSD is considered, three cases are investigated. In case A, the UPS is assumed and simulated. In case B, a PSD with a moderate variance is assumed. In case C, the variance of the PSD is further increased. For both case B and C, the Weibull distribution is used, only the distribution parameters are varied. The thermodynamic parameters for case A, B and C correspond to 10% SOC. In addition, to investigate the SOC dependence of the liquid diffusion and ease the data processing for the measurement data, the fourth case D will be investigated. In case D, the full order p2D impedance model is used to generate the impedance and all parameters are adopted from the case C except that the SOC is varied between 10% and 90% SOC. The common electrode parameters used for all cases are listed in Tables 5 and 6. The PSDs are generated using the following functions:

$$N(r) = \begin{cases} N_{\mathrm{p}}\delta\left(r - r_{\mathrm{p,D50}}\right) & \text{(UPS)} \\ N_{\mathrm{p}}\dfrac{b}{a}\left(\dfrac{x}{a}\right)^{b-1} e^{\left(-(x/a)^{b}\right)} & \text{(PSD)} \end{cases} \tag{60}$$

where a and b are distribution parameters and $r_{\mathrm{p,D50}}$ is the median of the particle size. The distribution parameters are determined by the following relations:

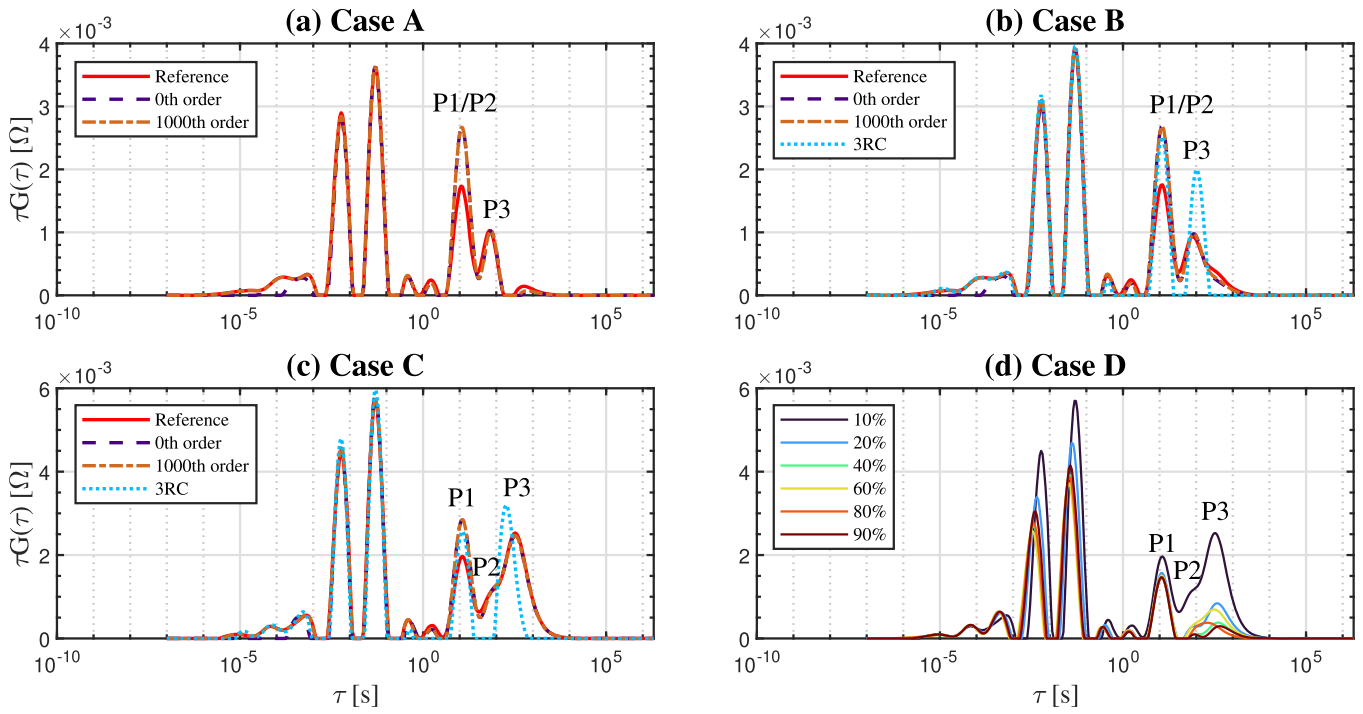

Fig. 4. Comparison of the the DRT spectra in various cases.

$$a = \frac{r_{\mathrm{p,D50}} - r_{\min}}{(\ln 2)^{\frac{1}{b}}} \tag{61}$$

$$N_{\mathrm{p}} = \frac{\epsilon_{\mathrm{s}}}{\int_0^{\infty} \frac{4}{3}\pi r^3 P(r) dr} \tag{62}$$

The generated UPS/PSDs for case A, B, C and D are shown in Fig. 3a–d. In both cases, the median of the particle radius is kept to the same value, which is namely the uniform particle size in case A.

The generated as well as the reconstructed impedances are shown in Fig. 3e–k. The comparison of the reference impedance with the impedance generated using the approximation 1 is plotted in Fig. 3e–g. No visible discrepancy can be observed, thus justifying the approximation 1 for the model development. Generally this approximation should be valid in most cases, as the time constants of the solid diffusion is usually orders of magnitude larger than that of the charge transfer and SEI. The simulation results for case D are shown in Fig. 3d and h.

To validate the theory on stage one dispersion, the impedance is reconstructed using Eq. (9) with the 0th order and 1000th order respectively. To test the performance of the 3RC approximation, the impedance is also reconstructed using the 3RC model. All reconstructed impedances together with the reference impedance is plotted in Fig. 3i–k. Besides, to better visualize the possible deviation between the various models, the corresponding DRT spectra are also calculated and shown in Fig. 4. In the low frequency area ($\tau \geq 1$ s) in Fig. 4, two or three peaks can be recognized and are marked with P1, P2 and P3. By comparing the time constant of each peak with the simulation parameters, we can conclude that P1 represents the diffusion in the electrolyte, P2 is related to the solid phase diffusion in the cathode and P3 is attributable to the solid phase diffusion in the anode.

In case A (see Fig. 3i), we can see that there exists an obvious discrepancy between the reference impedance and the 0th order reconstruction, and only a minor discrepancy can be observed between the reference impedance and the 1000th order reconstruction. We assume that the discrepancy has two causes, namely the high frequency dispersion and the liquid phase diffusion. This can be confirmed by analyzing the DRT spectra in Fig. 4, where discrepancy between the reference and the 0th order reconstructed DRT can only be observed at the peak P1/P2 representing the liquid diffusion and at the time constant 10^{-4} s where the high frequency dispersion appears. It should be mentioned here that the peaks for the solid diffusion in the anode and diffusion in the electrolyte are overlapping because of similar time constants. In such case, it's not possible to separate the impedance contribution from the electrolyte and the anode. Although the magnitude of diffusion impedance cannot be precisely calculated, the time constant can be accurately reflected.

In case B (see Fig. 3j), instead of assuming a uniform particle size, the solid particles in the electrode are modeled using a size distribution. We can see from Fig. 3f that the impedance is quite similar to that in case A and a relatively clear transition from the Warburg region into the capacitive region can be observed, except that the impedance is slightly scaled because of the changed volumetric interfacial area. In the capacitive region, impact of the PSD is also observable. Instead of a nearly vertical line and an ideal capacitive behavior, the impedance shows a slow transition into the ideal capacitive region, which is believed to be caused by the larger particles with higher diffusion time constants. The DRT spectra for case B (see Fig. 4b) is similar to that of case A (see Fig. 4a), the time constants of all peaks are very similar. It is worth noting that the peak P3 in Fig. 4b is slightly wider than that of case A and extends further into the area of higher time constants. We believe that this is caused by the PSD and is in accordance with the observation in Fig. 4, where a slow transition into the capacitive region is observed.

In case C (see Fig. 3k), the transition is further blurred and there exists a nearly smooth transition from the Warburg region into the capacitive region. In Fig. 4c, the peak P2 is somehow shifted to the area of higher time constants and can be observed. We assume that this is again caused by the PSD, similar to the diffusion in the cathode. Similarly, we can see that the peak with the largest time constant is extended for about an order of magnitude compared to case A and the time constant defined by the peak is also shifted. The simulation results clearly indicate that although the median of the particle size and the diffusion coefficients are the same for all the three cases, the position of the peaks is changed due to the effect of the PSD. Therefore, estimating the diffusion coefficients with the UPS assumption will cause possible errors, the magnitude of the errors depend on the variance of the PSD. In

Table 7
Description of the components in the coin cells.

Component	Description
Electrolyte	90 μL of 1M LiPF6 in 3:7 (wt:wt) ethylene carbonate (EC)/ethyl methyl carbonate (EMC) electrolyte (99.9% purity, Solvionic)
Separator	Celgard 2325
Counter-electrode	lithium-metal

case B and C, it can be seen that the 3RC model can well approximate the DRT spectra when the PSD is considered.

3.2. Application to commercial LIB

In this section, the developed theory will be applied to a commercial LIB, the diffusion coefficient of the Li-ion in the solid and liquid phase will be determined by evaluating the DRT spectra of the full cell and half cells.

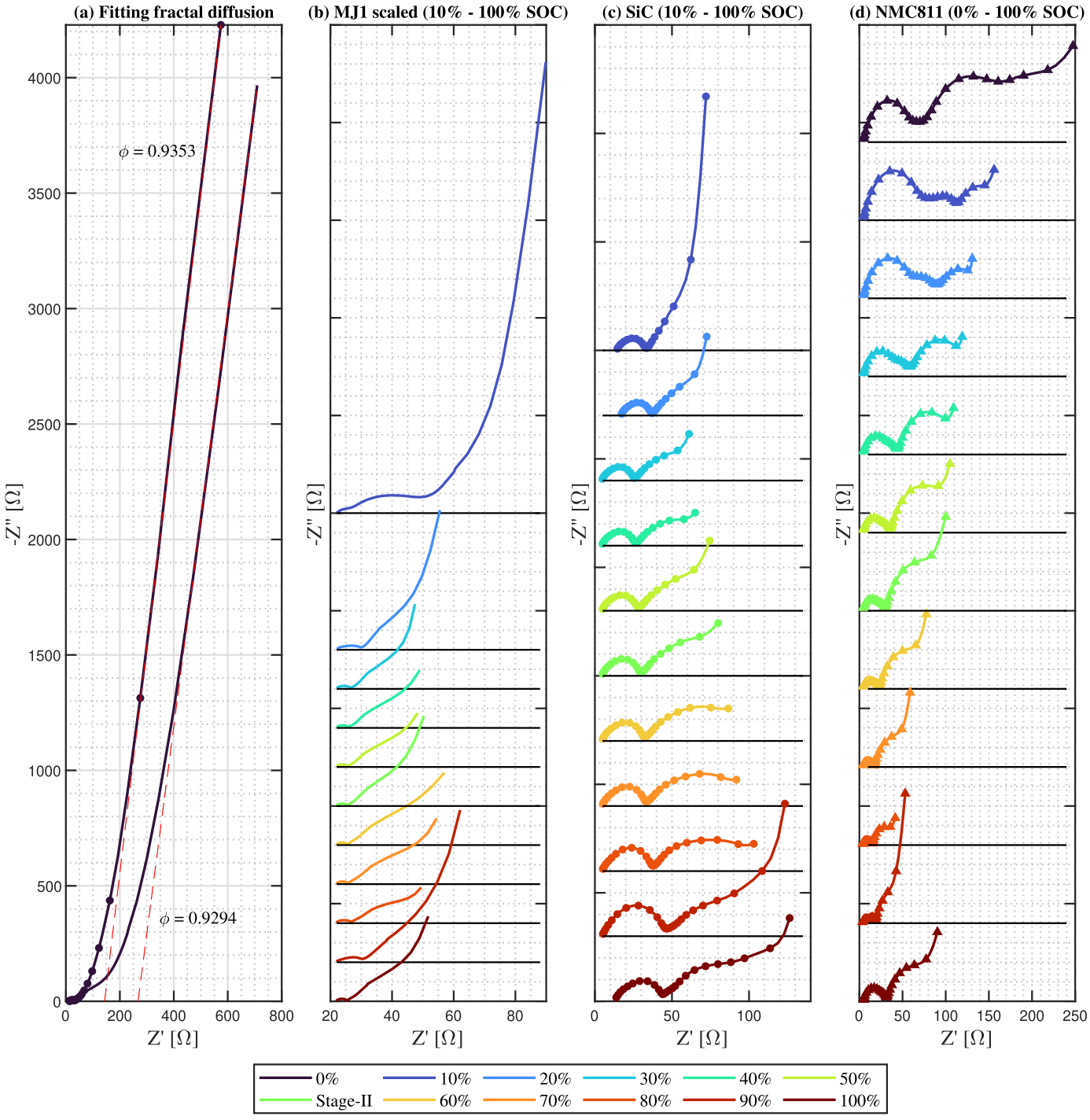

Fig. 5. Scaled impedance of the full cell and impedance of the half cells. (a): Impedance of the full cell and half cell with SiC at 0% SOC used to determine the fractal exponent; (b): full cell impedance at 10% (uppermost)–100% (lowermost) SOC; (c): impedance of half cell with SiC at 10% (uppermost)–100% (lowermost) SOC; (d): impedance of half cell with NMC811 at 0% (uppermost)–100% (lowermost) SOC.

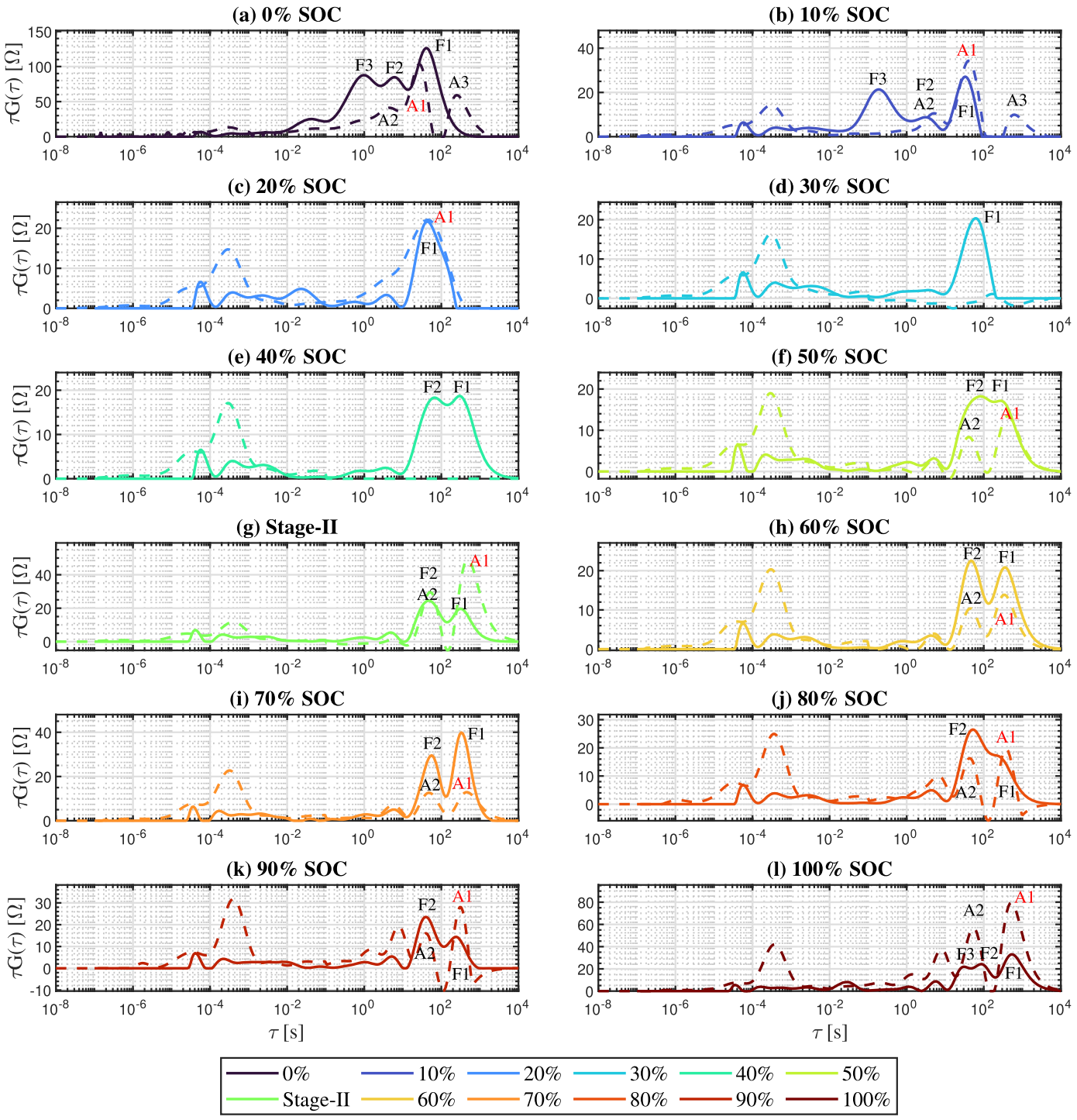

Fig. 6. DRT spectra of the full cell (solid line) and half cell (dashed line) with SiC at the lithiation state 2%–85.7%. The peaks that are attributed to the SiC are marked with red color. (For interpretation of the references to color in this figure legend, the reader is referred to the web version of this article.)

3.2.1. *Experimental*

The commercial cell investigated in this work is a 3.35 Ah NMC811/SiC LIB (INR18650-MJ1,LG Chem), which has been partly parametrized by Sturm et al. [26] and the fast kinetic processes have been investigated in our previous work as well [6]. First, the impedance of a full cell was measured at 0%–100% SOC with 10% increment under the temperature of 25 °C. Then another full cell from the same production lot was fully discharged and opened in an argon-filled glove-box, a piece of anode and cathode with a diameter of 10.95 mm were punched out of the electrode respectively. Because both sides of the electrodes were coated with active material, so one side of each sample was scraped off to minimize the influence of the backside coating. Then all the components were assembled into a 2032-type coin cell and a detailed description of the components can be found in Table 7. The assembled coin cells were rested for 24 h to improve wetting of the electrode and separator. Next, the coin cells were charged/discharged with a current of 800 μA to the lithiation state which corresponds to 100% SOC in the full cell. Then the impedance of the coin cells at the lithiation states which correspond to the 0–100% SOC in the full cell was measured under 25 °C. In addition, to characterize the diffusion of the Li-ions in graphite at the stage-II

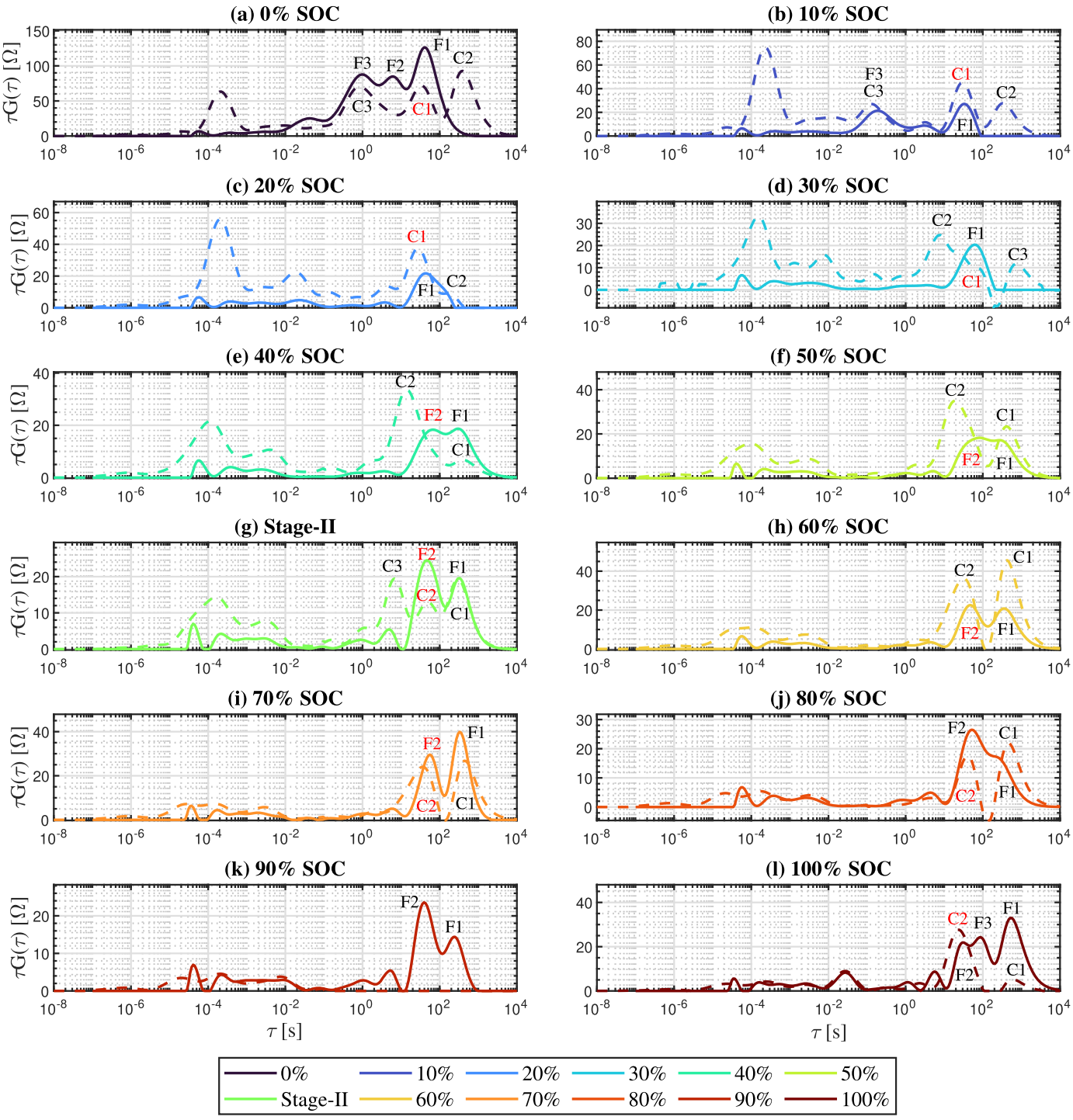

Fig. 7. DRT spectra of the full cell (solid line) and half cell (dashed line) with NMC811 at the lithiation state 22.2%–94.2%. The peaks that are attributed to the NMC811 are marked with red color. (For interpretation of the references to color in this figure legend, the reader is referred to the web version of this article.)

(LiC_{12}), the impedance of the full cell at ca. 56% SOC and the coin cells at the lithiation state which corresponds to the same SOC in the full cell were measured at 25 °C. Between each two SOC adjustments, the cells were relaxed for 6h.

For the GITT experiment, the same coin cells were used and the test was conducted at the same SOC points as for the impedance measurement. At each SOC point, the coin cell was first subjected to a charging current pulse with a duration of 600 s and an amplitude of 200 μA. Subsequently, the coin cell was relaxed for 2 h and then subjected to a discharging current pulse with the same duration and amplitude. The same procedure was repeated at each SOC point. At the upper voltage limit only discharging current pulse and at the lower voltage limit only charging current pulse was applied to protect the coin cell from overcharging and overdischarging.

The SOC adjustment, impedance measurement and GITT experiment were all performed on an electrochemical workstation (VMP3, Biologic), the frequency range of the impedance measurement was 10 kHz - 0.5 mHz for the full cell and 100 kHz - 0.5 mHz for the coin cells, the amplitude of the potential perturbation is 10 mV.

3.2.2. Results

In this section, the measured impedance data will be evaluated, the DRT spectra will be calculated and used to estimate the solid diffusion coefficients of Li-ions in the SiC and NMC811. In the rest of the work, for the purpose of brevity and consistency, we will refer to the lithiation state of the SiC and NMC811 in the half cells by using the corresponding SOC value in the full cell. The measured impedance data for half and full cells are shown in Fig. 5. The impedances at different SOCs are plotted against a shifted x-axis to achieve a better view and ease the comparison.

From Fig. 5, it can be clearly seen that while the full cell impedance is subjected to little influence from the liquid phase diffusion, the half cell impedance is strongly affected by the liquid phase diffusion, as in the low frequency range a big bump/half circle can be observed. For the SiC, except at the 0%–20% and 100% SOC, the rest of the impedance data is dominated by the liquid phase diffusion, which is superimposed on the solid diffusion impedance. For the NMC811, similar behavior can be observed, where at 0%–90% SOC the impedance is strongly influenced by the liquid diffusion.

Before the DRT spectra are calculated, a pre-processing step is carried out to characterize the fractal diffusion behavior in the solid phase and the fractal exponent is calculated. For the full cell, an obvious fractal diffusion can be recognized at the 0% SOC. In the capacitive region (see Fig. 5a), instead of an ideal capacitance with a 90° phase angle, a constant phase behavior with an angle smaller than 90° can be observed and the fractal exponent is calculated to be 0.9294. Similarly, the estimated fractal exponent is 0.9353 for the SiC electrode. Because the capacitive region of the NMC811 half cell impedance cannot guarantee a reliable estimation of the fractal exponent, no fractal diffusion is assumed for the NMC811. The calculated fractal exponents are further used for the DRT calculation. It is worth mentioning here that including the fractal exponents into the DRT calculation is crucial for the results, because without considering the fractal diffusion behavior the constant phase behavior will be misinterpreted as a part of the Warburg region and peaks with extremely high time constants and large magnitude will be obtained, which will lead to erroneous and unrealistic results.

Due to the fact that no precise information about the magnitude and time constants for the liquid phase diffusion is available, the influence of the liquid diffusion cannot be directly evaluated. Recalling the results of the synthetic simulation experiments, we can find that except for very high or low SOCs, the peak for the liquid diffusion only shows a tiny change, which can be approximately regarded as invariant in the mid SOC range. This feature can be used to remove the contribution of the liquid phase diffusion effectively even without precise information about the liquid phase diffusion. First, one specific SOC value is chosen for each half cell at which the impedance has the least solid phase diffusion impedance and the diffusion is dominated by the liquid diffusion. Then the DRT spectrum of the chosen SOC is subtracted from all DRT spectra in the mid SOC range to derive the approximated spectra without the influence of the liquid diffusion.

For the SiC, the impedance at 40% SOC is chosen as the reference and the DRT spectrum at 40% is subtracted from the spectra at the 30%–90% SOC. For the NMC811, the impedance at 90% SOC is chosen and the DRT spectrum at 90% SOC is subtracted from the spectra at 30%–90% SOC. The resulting DRT spectra are shown in Figs. 6 and 7 for the SiC and NMC811 respectively. In the following section, the resulting DRT spectra will be analyzed, the peak attribution will be performed and the solid diffusion coefficients will be estimated.

0% SOC For the SiC, a dominating solid diffusion impedance can be seen (see Fig. 5a) and in the DRT spectra a series of peaks with decreasing magnitude and time constants can be observed, which is a typical sign of solid diffusion. As a result, peak A1 is attributed to the solid diffusion in the SiC, the peaks F2 and A2 are caused by the frequency dispersion of the solid diffusion and will be excluded from further analysis. Peak F3 is missing in the SiC spectra but appears in the full cell, we will return to the attribution of the peak F3 later. Peak A3 only appears in the half cell, so it is attributed to the liquid diffusion in the half cell. It is worth noticing that peak A1 doesn't fully coincide with the peak F1, we assume the deviation arises from the contribution of the NMC811, this conclusion will be confirmed later. For the NMC811, C3 coincides with the peak F3, considering that this peak is later shifted to the area of smaller time constants and the magnitude also decreases, we attributed F3 and C3 to the charge transfer in the NMC811, which has been investigated and confirmed in our previous work as well [6]. Peak C1 and F1 share the same time constant, so C1 is attributed to the solid diffusion in the NMC811, thus explaining the discrepancy between the peak A1 and F1. C2 has a similar time constant to that of A3, so it is attributed to the liquid diffusion in the half cell.

10% SOC Similar to 0% SOC, the SiC half cell shows a significant solid diffusion behavior (see Fig. 5c), as a result, the peaks F1 and A1 are attributed to the solid diffusion in the SiC. For the NMC811 (see Fig. 5d), the magnitude of the peak C1 decreases, which is in accordance with the impedance change of the NMC811 half cell. Hence, peak C1 is attributed to the NMC811. In both half cells, the magnitude of peak A1 and C1 is larger than that of the peak F1, hence, we believe that the liquid diffusion in the half cell has also contributed to the peak A1/C1.

20% SOC From the impedance plot in Fig. 5c it can be seen that solid diffusion impedance for the SiC further decreases (see the decreased Warburg impedance), which is most likely caused by the decreasing dOCV. In the DRT spectra, the peak A1 and F1 are almost overlapping (see Fig. 6c), so the peak A1/F1 is attributed to the solid diffusion in the SiC. For the NMC811 (see Fig. 7c), the peaks C1 and F1 share the same time constant, hence they are also attributed to the solid diffusion in the NMC811.

30% SOC Because the DRT spectrum at the 30% SOC has been chosen as the reference for the SiC, no information about solid diffusion in the SiC is available. For the NMC811 (see Fig. 7d), F1 and C1 have the same time constant, as a result, F1/C1 is attributed to the solid diffusion in the NMC811, while C2/C3 is attributed to the rest contribution from the liquid diffusion.

40%–90% SOC In this SOC range, all DRT spectra have a similar form and we choose to perform the peak attribution altogether for all these SOC values. In the DRT spectra of either material (see Figs. 6e–k and 7 e-k), the peaks A1, A2, C1, C2, F1 and F2 are existent at the same time, making a direct peak attribution rather difficult. Therefore, we choose to conduct the peak attribution in an indirect way.

In the 40%–90% SOC range, we can notice that the peak F1 and F2 all have comparable magnitude, according to Eq. (27), for the magnitude of the prominent peak the following relation holds:

$$H_1 \propto \frac{\left(-\frac{\partial U}{\partial c_s}\right)}{D_s} \tag{63}$$

where H_1 is the magnitude of the prominent peak. This relation indicates if two processes have comparable peak magnitude, then the process with higher diffusion coefficient should also have a higher dOCV value. In our case, the dOCV of SiC in the 40%–90% SOC range is much smaller than that of the NMC811, which means the SiC should also have a smaller solid diffusivity and a higher time constant. As a result, we attribute F2/C2 to the solid diffusion in the NMC811 and F1/A1 to the solid diffusion in the SiC. It is worth noticing that at the stage-II, the dOCV of the SiC is very close to that of the NMC811. Under such condition, if the diffusion coefficient (time constant) doesn't change, then the peak magnitude should increase significantly. At stage-II, it can be observed that peak A1 has increased significantly, thus it is also attributed to the SiC.

100% SOC By inspecting the DRT spectra of NMC811 (see Fig. 7l), we can easily attribute the peak C2/F2 to the solid diffusion in the NMC811. Then we can exclude the possibility that the peak F3 is attributed to the solid diffusion in the SiC, because the dOCV value and the time constant (no matter for F1/F3) both increase, as a result, the peak magnitude should increase as well. Hence, the peak A1/F1 is attributed to the solid diffusion in the SiC.

The results for the peak attribution and time constants for the SiC and

Table 8
Summary of the peak attribution.

SOC	SiC		NMC811	
	Peak attribution	Time constants [s]	Peak attribution	Time constants [s]
0%	A1	27	C1	39
10%	A1	39	C1	32
20%	A1	42	C1	27
30%	N.A.	N.A.	C1	62
40%	N.A.	N.A.	F2	62
50%	A1	359	F2	39
60%	A1	298	F2	32
70%	A1	393	F2/C2	35
80%	A1	393	C2	47
90%	A1	327	N.A.	N.A.
100%	A1	519	C2	27
stage-II	A1	431	F2/C2	38

NMC811 are summarized in the following Table 8.

After the peak attribution has been performed and the time constants for the peaks have been read, the solid diffusion coefficients can be estimated. Heenan et al. investigated the solid particle geometry and the particle size distribution of the same cell used in the present work [28]. According to the measurement of the particle size distribution, both the SiC and NMC811 have a wide particle size distribution and thus a large particle radius variance. As a result, we use the developed 3RC assumption to estimate the solid diffusion coefficients. Besides, the fractal diffusion behavior is also accounted for when estimating the diffusion coefficients. The estimated solid diffusion coefficients with DRT and GITT for the SiC and NMC811 are shown in Fig. 8.

For the SiC, it can be observed that the solid diffusion coefficients estimated at 0.2%, 8.7%, 47.8% (stage-II) and 85.2% lithiation state with both DRT and GITT are close to each other. The estimated values at the stage-II and 85.2% lithiation state are ca. 1.8×10^{-10} $cm^2\,s^{-1}$ and 1×10^{-10} $cm^2\,s^{-1}$ respectively, which are comparable to the values (1.8×10^{-10} $cm^2\,s^{-1}$ and 0.5×10^{-10} $cm^2\,s^{-1}$) measured by Umegaki et al. [29] with the μ^+SR method. Similar values have also been found for the same lithiation states in Cabañero et al. [7], Ecker et al. [30], Schmalstieg and Sauer [31]. Interestingly, the diffusion coefficients estimated at other lithiation states using GITT are much lower than that using the DRT. Furthermore, the estimated values with GITT using the charging and discharging current pulse generally follow a similar pattern. The shown pattern resembles the differential open circuit voltage (dOCV) of the anode, which has been observed by Cabañero et al. as well [7]. We believe that this phenomenon can be explained by analyzing the dOCV and the influence of the liquid phase diffusion. To ease the analysis, the dOCV of the same material is plotted in the same figure in Fig. 8.

It can be seen in Fig. 8 that at each lithiation state where the estimated values using DRT and GITT coincide with each other, a peak can be observed on the dOCV curve. A peak on the dOCV curve indicates that when the electrode is perturbed at this lithiation state, the electrode will give a higher voltage response compared to other lithiation states. The higher voltage response will manifest itself as a higher solid diffusion impedance (see Fig. 5) and a higher diffusion-induced overpotential in the GITT experiment. On the other hand, during the GITT experiment, the overpotential will be inevitably influenced by the liquid diffusion, which is invisible in GITT experiment but can be well observed in impedance spectra (see Fig. 5). As a result, the total diffusion overpotential is consisted of the contribution of the solid and liquid diffusion:

$$\Delta E_{t,diff} = \Delta E_{t,diff,l} + \Delta E_{t,diff,s} \tag{64}$$

At the lithiation states with higher dOCV values, the $\Delta E_{t,diff,s}$ is non-negligible or is even dominating, the estimated diffusion coefficients are close to the true values. On the contrary, at the lithiation states with low dOCV values, $\Delta E_{t,diff,l} \gg \Delta E_{t,diff,s}$ so that the following relation is valid:

$$D_{s,GITT} \propto \left(\frac{\Delta E_s}{\Delta E_{t,diff,l} + E_{t,diff,s}}\right)^2 \ll \left(\frac{\Delta E_s}{\Delta E_{t,diff,s}}\right)^2 \tag{65}$$

This equation explains the phenomenon that the solid diffusion coefficients measured at lithiation states with higher dOCV values are much higher than that measured at lithiation states with low dOCV values. As a result, the measured diffusion coefficients with GITT follow the pattern of the dOCV curve, which has also been observed in Cabañero et al. [7].

For the NMC811, the similar phenomenon can be seen. At the 22.2%, 36.6% and 51% lithiation states with a higher dOCV value, the diffusion coefficients estimated with the DRT and GITT have similar values. At other lithiation states, the values estimated with GITT are much lower than that with the DRT as expected. The measured solid diffusion coefficients in the present work are comparable to the values found in Chen et al. [32], Noh et al. [33].

In summary, the DRT method can be applied to determine the solid diffusion coefficient even if the liquid diffusion exists, while the GITT is only able to estimate the diffusion coefficient when the diffusion is not or less affected by the liquid diffusion. At the lithiation states with low dOCV values, the diffusion coefficients will be strongly underestimated due to the influence of the liquid diffusion.

4. Conclusions

In the present work, a theory is proposed to investigate the diffusion processes in a LIB using the DRT spectrum and with a physics-based

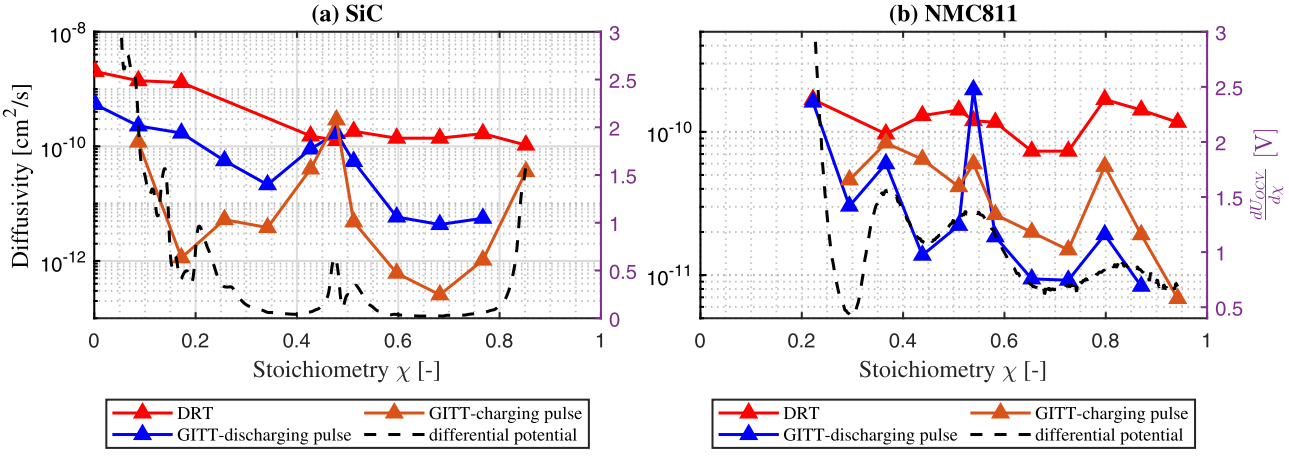

Fig. 8. Calculated solid diffusion coefficient of Li-ions in (a): SiC and (b): NMC811 at different lithiation states.

impedance model. Furthermore, an analytical expression for the DRT spectrum is proposed, which has related the electrochemical parameters to the DRT spectrum in an explicit way. Subsequently, simulation and lab experiments are conducted to validate the proposed model and the solid diffusivity of SiC and NMC811 is estimated using the developed model. Besides, GITT experiment has been conducted to estimate the solid diffusion coefficients for the SiC and NMC811. The results indicate that the GITT can significantly underestimate the solid diffusion coefficients when the electrode is subjected to the influence from the liquid diffusion and the dOCV value is low. Compared to the GITT which is based on the voltage measurement in time domain, DRT is based on the time constant and does not directly rely on the voltage measurement in time domain, even if the liquid diffusion exists, the solid diffusion coefficient can be reliably estimated.

CRediT authorship contribution statement

Yulong Zhao: Conceptualization, Methodology, Software, Investigation, Validation, Data curation, Formal analysis, Writing – original draft, Project administration. **Simon Kücher:** Investigation, Resources, Writing – review & editing. **Andreas Jossen:** Supervision, Writing – review & editing.

Declaration of Competing Interest

The authors declare that they have no known competing financial interests or personal relationships that could have appeared to influence the work reported in this paper.

Acknowledgment

This research is funded by the China Scholarship Council (CSC), the author gratefully thanks for the support and funding from CSC.

Appendix A. Derivation of series expansion for the diffusion impedance

A1. Planar solid particle

Obviously the impedance expression for planar solid particle has a pole of zero, the corresponding expansion coefficient is calculated as:

$$b_0 = \lim_{s\to 0} s\frac{\coth(\sqrt{s\tau})}{\sqrt{s\tau}} = \frac{1}{\tau_0} \tag{A.1}$$

The higher order poles are determined by solving the following equation:

$$\sinh\sqrt{a_n\tau_0} = 0 \Rightarrow a_n = -\frac{n^2\pi^2}{\tau_0} \qquad (n = 1, 2, 3, \ldots) \tag{A.2}$$

The corresponding expansion coefficients are calculated with the same principle:

$$b_n = \lim_{s\to a_n}(s - a_n)\frac{\coth(\sqrt{s\tau})}{\sqrt{s\tau}} = \frac{2}{\tau_0} \tag{A.3}$$

As a result the expansion can be rewritten as:

$$\frac{\coth(\sqrt{s\tau})}{\sqrt{s\tau}} = \frac{b_0}{s} + \sum_{n=1}^{\infty}\frac{b_n}{s - a_n} = \frac{1}{s\frac{1}{b_0}} + \sum_{n=1}^{\infty}\left(-\frac{b_n}{a_n}\right)\frac{1}{1 + s\left(-\frac{1}{a_n}\right)} \tag{A.4}$$

If the capacitance term is subtracted from the equation above and the DRT is conducted, the following equation can be obtained:

$$G(\tau) = \sum_{n=1}^{\infty} -\frac{b_n}{a_n}\delta\left(\tau + \frac{1}{a_n}\right) \tag{A.5}$$

The dispersion time constants given as:

$$\tau_n = -\frac{1}{a_n} = \frac{\tau_0}{n^2\pi^2} \tag{A.6}$$

The dispersion magnitude R_n is calculated as:

$$R_n = -\frac{b_n}{a_n} = \frac{2}{n^2\pi^2} \tag{A.7}$$

A2. Cylindrical solid particle

Like the planar solid particle, for cylindrical particle there exists also a pole of zero, the corresponding coefficient is given as:

$$b_0 = \lim_{s\to 0} s\frac{I_0\left(\sqrt{s\tau_0}\right)}{\sqrt{s\tau_0}I_1\left(\sqrt{s\tau_0}\right)} = \frac{2}{\tau_0} \tag{A.8}$$

The higher order poles are calculated by solving the following equation:

$$I_1(\sqrt{s\tau_0}) = 0 \tag{A.9}$$

Because the modified Bessel function above has an imaginary argument, it cannot be solved conveniently, therefore the following relation is applied to simplify the equation:

$$I_\alpha(ix) = i^{-\alpha} J_\alpha(-x) \tag{A.10}$$

where J_α is the Bessel function of the order α. As a result Eq. (A.9) can be transformed into the following equation:

$$J_1\left(-\sqrt{|a_n|\tau_0}\right) = 0 \tag{A.11}$$

The equation above can be readily solved using a look-up table for zeros of Bessel functions. If we assume the zeros of the Bessel function to be λ_n, then the poles can be expressed as:

$$a_n = -\frac{\lambda_n^2}{\tau_0} \tag{A.12}$$

The expansion coefficients are calculated as:

$$b_n = \lim_{s\to a_n}(s-a_n)\frac{I_0\left(\sqrt{s\tau_0}\right)}{\sqrt{s\tau_0}I_1\left(\sqrt{s\tau_0}\right)} = \frac{2}{\tau_0} \tag{A.13}$$

With the same procedures as shown for planar particles, the dispersion time constants and magnitude are given as:

$$\tau_n = -\frac{1}{a_n} = \frac{\tau_0}{\lambda_n^2} \tag{A.14}$$

$$R_n = -\frac{b_n}{a_n} = \frac{2}{\lambda_n^2} \tag{A.15}$$

A3. Spherical solid particles

The impedance expression has a pole of zero, and the corresponding coefficient is calculated as:

$$b_0 = \lim_{s\to 0} s\frac{\tanh\left(\sqrt{s\tau_0}\right)}{\sqrt{s\tau_0}-\tanh\left(\sqrt{s\tau_0}\right)} = \frac{3}{\tau_0} \tag{A.16}$$

The higher order poles are determined by solving the following equation:

$$\sqrt{a_n\tau_0} - \tanh\left(\sqrt{a_n\tau_0}\right) = 0 \tag{A.17}$$

Note that $\tanh(ix) = i\tan(x)$, the equation above can be simplified to:

$$\sqrt{|a_n|\tau_0} - \tan\left(\sqrt{|a_n|\tau_0}\right) = 0 \tag{A.18}$$

By using look-up tables or numerical algorithms the equation can be solved conveniently. If we assume the solutions of equation $\tan(x) = x$ to be λ_n, then the poles are given as:

$$a_n = -\frac{\lambda_n^2}{\tau_0} \tag{A.19}$$

The expansion coefficients are:

$$b_n = \lim_{s\to a_n}(s-a_n)\frac{\tanh\left(\sqrt{s\tau_0}\right)}{\sqrt{s\tau_0}-\tanh\left(\sqrt{s\tau_0}\right)} = \frac{2}{\tau_0} \tag{A.20}$$

Similarly, the dispersion time constants and magnitude are calculated as:

$$\tau_0 = -\frac{1}{a_n} = \frac{\tau_0}{\lambda_n^2} \tag{A.21}$$

$$R_n = -\frac{b_n}{a_n} = \frac{2}{\lambda_n^2} \tag{A.22}$$

A4. Derivation of dispersion coefficients

According to the theorem on residue of composition function [34], the expansion coefficients can be calculated in the following way:

$$b_n = Res\left(Z_e\left(Y_{v,loc}\right), A_n\right) Y_{v,loc}(a_n)' \tag{A.23}$$

where a_n and b_n are the corresponding expansion pole and coefficient of each process. When the frequency is not extremely low and the capacitive effect can be neglected, the particle impedance can be approximated as a sum of RC elements, the admittance is thus expressed as:

$$Y_{v,loc} = \left(\sum_{i=1}^{\infty}\frac{R_i}{1+s\tau_i}\right)^{-1} \tag{A.24}$$

If we consider the k-th RC element, the impedances of all the RC elements with smaller time constants can be approxiamted as an ohmic resistance R_{k-1} and the that of the RC elements with larger time constants can be approximated to be zero, therefore we have:

$$Y_{v,loc} = \left(R_{k-1} + \frac{R_k}{1 + s\tau_k} \right)^{-1} \tag{A.25}$$

The pole corresponding to a_k is obtained by solving the following equation:

$$-\frac{k^2\pi^2}{l_e^2\left(\frac{1}{\kappa}+\frac{1}{\sigma}\right)} = \left(\sum_{i=1}^{\infty} \frac{R_i}{1 + s\tau_i} \right)^{-1} \tag{A.26}$$

Then the coefficient is calculated to be:

$$b_k = \frac{B_k R_k \tau_k}{\left(R_k + R_{k-1} - R_{k-1} a_k \tau_k\right)^2} \tag{A.27}$$

The equation above shows that the dispersion coefficients decreases with the corresponding time constants. Noting that usually the diffusion time constants are orders of magnitude greater than that of charge transfer and SEI process, the dispersion for diffusion can be neglected in practice.

References

[1] A. Lasia, Electrochemical impedance spectroscopy and its applications. Modern Aspects of Electrochemistry, Springer, 2002, pp. 143–248.
[2] J.R. Macdonald, E. Barsoukov, Impedance spectroscopy: theory, experiment, and applications, History 1 (8) (2005) 1–13.
[3] B.A. Boukamp, Derivation of a distribution function of relaxation times for the (fractal) finite length warburg, Electrochim. Acta 252 (2017) 154–163.
[4] B.A. Boukamp, A. Rolle, Use of a distribution function of relaxation times (DFRT) in impedance analysis of SOFC electrodes, Solid State Ionics 314 (2018) 103–111.
[5] J. Illig, J.P. Schmidt, M. Weiss, A. Weber, E. Ivers-Tiffée, Understanding the impedance spectrum of 18650 lifePO4-cells, J. Power Sources 239 (2013) 670–679.
[6] Y. Zhao, V. Kumtepeli, S. Ludwig, A. Jossen, Investigation of the distribution of relaxation times of a porous electrode using a physics-based impedance model, J. Power Sources 530 (2022) 231250.
[7] M.A. Cabañero, N. Boaretto, M. Röder, J. Müller, J. Kallo, A. Latz, Direct determination of diffusion coefficients in commercial li-ion batteries 165 (5) (2018) A847–A855, https://doi.org/10.1149/2.0301805jes.
[8] D.W. Dees, S. Kawauchi, D.P. Abraham, J. Prakash, Analysis of the galvanostatic intermittent titration technique (GITT) as applied to a lithium-ion porous electrode 189 (1) (2009) 263–268, https://doi.org/10.1016/j.jpowsour.2008.09.045.
[9] K.M. Shaju, G.V. Subba Rao, B.V.R. Chowdari, Li ion kinetic studies on spinel cathodes, Li($M_{1/6}Mn_{11/6}$)O_4 (M = Mn, Co, CoAl) by GITT and EIS 13 (1) (2003) 106–113, https://doi.org/10.1039/B207407A.
[10] J.H. Park, H. Yoon, Y. Cho, C.-Y. Yoo, Investigation of lithium ion diffusion of graphite anode by the galvanostatic intermittent titration technique 14 (16) (2021), https://doi.org/10.3390/ma14164683.34443205
[11] C.-H. Chen, F. Brosa Planella, K. O'Regan, D. Gastol, W.D. Widanage, E. Kendrick, Development of experimental techniques for parameterization of multi-scale lithium-ion battery models 167 (8) (2020) 080534, https://doi.org/10.1149/1945-7111/ab9050.
[12] S.D. Kang, J.J. Kuo, N. Kapate, J. Hong, J. Park, W.C. Chueh, Galvanostatic intermittent titration technique reinvented: part II. Experiments 168 (12) (2021) 120503, https://doi.org/10.1149/1945-7111/ac3939.
[13] C.J. Wen, B.A. Boukamp, R.A. Huggins, W. Weppner, Thermodynamic and mass transport properties of "LiAl " 126 (12) (1979) 2258–2266, https://doi.org/10.1149/1.2128939.
[14] M. Doyle, T.F. Fuller, J. Newman, Modeling of galvanostatic charge and discharge of the lithium/polymer/insertion cell, J. Electrochem. Soc. 140 (6) (1993) 1526.
[15] M. Doyle, J. Newman, Modeling the performance of rechargeable lithium-based cells: design correlations for limiting cases, J. Power Sources 54 (1) (1995) 46–51.
[16] M. Doyle, J. Newman, A.S. Gozdz, C.N. Schmutz, J.-M. Tarascon, Comparison of modeling predictions with experimental data from plastic lithium ion cells, J. Electrochem. Soc. 143 (6) (1996) 1890–1903.
[17] G.B. Arfken, H.J. Weber, Mathematical methods for physicists, 1999.
[18] J. Song, M.Z. Bazant, Electrochemical impedance imaging via the distribution of diffusion times, Phys. Rev. Lett. 120 (11) (2018) 116001.
[19] J. Huang, J. Zhang, Theory of impedance response of porous electrodes: simplifications, inhomogeneities, non-stationarities and applications, J. Electrochem. Soc. 163 (9) (2016) A1983.
[20] J. Song, M.Z. Bazant, Effects of nanoparticle geometry and size distribution on diffusion impedance of battery electrodes, J. Electrochem. Soc. 160 (1) (2012) A15.
[21] E. Quattrocchi, T.H. Wan, A. Curcio, S. Pepe, M.B. Effat, F. Ciucci, A general model for the impedance of batteries and supercapacitors: the non-linear distribution of diffusion times, Electrochim. Acta 324 (2019) 134853.
[22] T.H. Wan, M. Saccoccio, C. Chen, F. Ciucci, Influence of the discretization methods on the distribution of relaxation times deconvolution: implementing radial basis functions with DRTtools, Electrochim. Acta 184 (2015) 483–499.
[23] X. Zhou, J. Huang, Z. Pan, M. Ouyang, Impedance characterization of lithium-ion batteries aging under high-temperature cycling: importance of electrolyte-phase diffusion, J. Power Sources 426 (2019) 216–222.
[24] G. Sikha, R.E. White, Analytical expression for the impedance response of an insertion electrode cell, J. Electrochem. Soc. 154 (1) (2006) A43.
[25] G. Sikha, R.E. White, Analytical expression for the impedance response for a lithium-ion cell, J. Electrochem. Soc. 155 (12) (2008) A893.
[26] J. Sturm, A. Rheinfeld, I. Zilberman, F.B. Spingler, S. Kosch, F. Frie, A. Jossen, Modeling and simulation of inhomogeneities in a 18,650 nickel-rich, silicon-graphite lithium-ion cell during fast charging, J. Power Sources 412 (2019) 204–223.
[27] L.O. Valøen, J.N. Reimers, Transport properties of LiPF6-based Li-ion battery electrolytes, J. Electrochem. Soc. 152 (5) (2005) A882.
[28] T. Heenan, A. Jnawali, M. Kok, T.G. Tranter, C. Tan, A. Dimitrijevic, R. Jervis, D. Brett, P.R. Shearing, An advanced microstructural and electrochemical datasheet on 18,650 Li-ion batteries with nickel-rich NMC811 cathodes and graphite-silicon anodes, J. Electrochem. Soc. 167 (14) (2020) 140530.
[29] I. Umegaki, S. Kawauchi, H. Sawada, H. Nozaki, Y. Higuchi, K. Miwa, Y. Kondo, M. Månsson, M. Telling, F.C. Coomer, et al., Li-ion diffusion in li intercalated graphite C_6 Li and C_{12} Li probed byμ+ SR, Phys. Chem. Chem. Phys. 19 (29) (2017) 19058–19066.
[30] M. Ecker, S. Käbitz, I. Laresgoiti, D.U. Sauer, Parameterization of a physico-chemical model of a lithium-ion battery: II. Model validation, J. Electrochem. Soc. 162 (9) (2015) A1849.
[31] J. Schmalstieg, D.U. Sauer, Full cell parameterization of a high-power lithium-ion battery for a physico-chemical model: part II. Thermal parameters and validation, J. Electrochem. Soc. 165 (16) (2018) A3811.
[32] C.-H. Chen, F.B. Planella, K. O'regan, D. Gastol, W.D. Widanage, E. Kendrick, Development of experimental techniques for parameterization of multi-scale lithium-ion battery models, J. Electrochem. Soc. 167 (8) (2020) 080534.
[33] H.-J. Noh, S. Youn, C.S. Yoon, Y.-K. Sun, Comparison of the structural and electrochemical properties of layered Li [nixcoymnz] O_2 (X= 1/3, 0.5, 0.6, 0.7, 0.8 and 0.85) cathode material for lithium-ion batteries, J. Power Sources 233 (2013) 121–130.
[34] R. Remmert, Theory of Complex Functions vol. 122, Springer Science & Business Media, 1991.